Microkinetic modeling with size-dependent and adsorbate–adsorbate interactions for the direct synthesis of H_2O_2 over Pd nanoparticles

Zhao, J., Yao, Z., Bunting, R. J., Hu, P., & Wang, J. (2023). Microkinetic modeling with size-dependent and adsorbate–adsorbate interactions for the direct synthesis of H_2O_2 over Pd nanoparticles. *ACS Catalysis*, *13*(22), 15054-15073. https://doi.org/10.1021/acscatal.3c03893

Published in:
ACS Catalysis

Document Version:
Publisher's PDF, also known as Version of record

Queen's University Belfast - Research Portal:
Link to publication record in Queen's University Belfast Research Portal

ACS Catalysis

pubs.acs.org/acscatalysis
Research Article

Microkinetic Modeling with Size-Dependent and Adsorbate−Adsorbate Interactions for the Direct Synthesis of H_2O_2 over Pd Nanoparticles

Jinyan Zhao,[⊥] Zihao Yao,*[,⊥] Rhys J. Bunting, P. Hu,* and Jianguo Wang*

Cite This: *ACS Catal.* 2023, 13, 15054−15073
Read Online

ACCESS | Metrics & More | Article Recommendations | Supporting Information

ABSTRACT: As a bottleneck in the direct synthesis of hydrogen peroxide, the development of an efficient palladium-based catalyst has garnered great attention. However, elusive active centers and reaction mechanism issues inhibit further optimization of its performance. In this work, advanced microkinetic modeling with the adsorbate−adsorbate interaction and nanoparticle size effect based on first-principles calculations is developed. A full mechanism uncovering the significance of adsorbate−adsorbate interaction is determined on Pd nanoparticles. We demonstrate unambiguously that Pd(100) with main coverage species of O_2 and H is beneficial to H_2O_2 production, being consistent with experimental operando observation, while H_2O forms on Pd(111) covered by O species and Pd(211) covered by O and OH species. Kinetic analyses further enable quantitative estimation of the influence of temperature, pressure, and particle size. Large-size Pd nanoparticles are found to achieve a high H_2O_2 reaction rate when the operating conditions are moderate temperature and higher oxygen partial pressure. We reveal that specific facets of the Pd nanoparticles are crucial factors for their selectivity and activity. Consistent with the experiment, the production of H_2O_2 is discovered to be more favorable on Pd nanoparticles containing Pd(100) facets. The ratio of H_2/O_2 induces substantial variations in the coverage of intermediates of O_2 and H on Pd(100), resulting in a change in product selectivity.

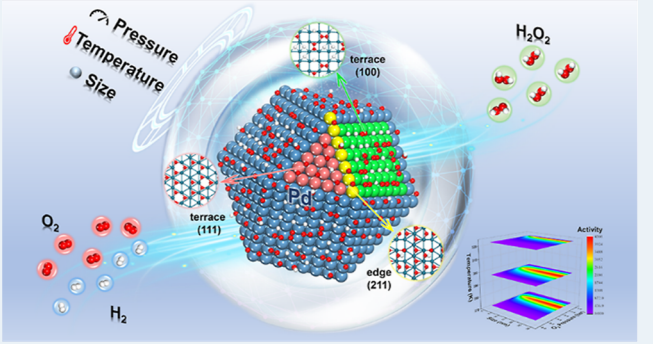

KEYWORDS: *direct synthesis of hydrogen peroxide, DFT, size effect, microkinetic modeling, adsorbate−adsorbate interaction*

1. INTRODUCTION

As one of a hundred significant chemical raw materials, hydrogen peroxide (H_2O_2) has a wide range of applications in the industry,[1−4] such as pulp/paper bleaching, food disinfection, wastewater treatment, and synthesis of propene epoxide (PO). The predominant industrial production of H_2O_2 is through anthraquinone auto-oxidation (AO). Overall, this process consists of the anthraquinone catalyst that is hydrogenated and oxidized sequentially, which was optimized by Riedl and Pfleidere,[5] enabling continuous work on the production line by preventing an explosion area of mixture gas (H_2 and O_2). However, the AO process is known to be indirect, energy-demanding, and waste-intensive. Therefore, a more eco-friendly production process has been proposed to avoid the weakness of the AO process: direct synthesis of hydrogen peroxide (DSHP) as a research hotspot has the advantages of green environmental protection, a high atom utilization rate, and ready-to-use immediately after H_2O_2 production.[6−10] But its efficiency still falls short of expectations, and the inherent flammability hazard is associated with mixing H_2 with O_2. In addition, direct synthesis of H_2O_2 is only achievable with costly pure O_2 in excess but not with freely available air, resulting in higher production costs.[11] The price of reactors and compressors for the direct synthesis of hydrogen peroxide can be decreased by reducing the reaction pressure and using more active and selective catalysts to compete with the AO process.

Among the extensively studied topics, Pd nanoparticles have been identified as the most effective catalyst for the direct synthesis of hydrogen peroxide. It has been revealed that catalytic activity and selectivity strongly depend on the size of the Pd nanoparticles.[12−22] For instance, Kim et al.[23] found that the production rate of hydrogen peroxide declined along with the decrease in the Pd nanoparticle size. Subsequently, Pd nano-octahedrons in various sizes (7.5−18 nm) were synthesized by Lee and co-workers,[14] and the smallest octahedron (7.5 nm) has the lowest selectivity and productivity of H_2O_2. It has long been

Received: August 17, 2023
Revised: October 25, 2023
Accepted: October 26, 2023
Published: November 6, 2023

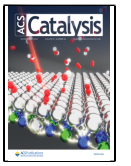

https://doi.org/10.1021/acscatal.3c03893
ACS Catal. 2023, 13, 15054−15073

speculated that the catalysts with smaller particle sizes have more sites that are coordinatively more unsaturated (defects, edges, and corners) where the O−O bond is dissociated and the formation of H_2O is promoted.[24] On the other hand, Pd nanoparticles for the direct synthesis of H_2O_2 are also effective for their subsequent decomposition (this process is facile and irreversible), which is known to be the bottleneck, hindering the overall DSHP process. Based on the theoretical work,[25−27] undesirable side reactions (H_2O formation and H_2O_2 decomposition) are more likely to occur on sites that are coordinatively more unsaturated, such as corners or edges. However, it was found experimentally that the Pd nanoparticles of subnano size (smaller than 2 nm) supported on hydroxyapatite presented a better performance for H_2O_2 production.[10,12] This phenomenon can be attributed to the fact that PdO_x/Pd interfaces on subnano-sized particles are formed, which could suppress the dissociation of O_2. Additionally, the H_2O_2 performance of Pd nanoparticles is highly susceptible to the reaction environment (H_2 and O_2 pressures,[6,28,29] selection of the solvents,[30,31] identity of the diluent gas,[32] addition of promoters,[33−35] and reaction temperature[36]) contributing to the distribution of various surface species. In essence, the active site changes constantly in the reaction process (poisoned or transformed into other active sites), resulting in the activity and selectivity changes of H_2O_2. Although some investigations have speculated that the performances of the catalysts are related to active sites,[37−44] the origin of the particle-size-dependent activity and selectivity is still puzzling.

Theoretical studies are required to drive the further development of this system. Usually, active sites of catalysts are simulated using clusters or periodic surfaces.[13,25,27,45,46] For example, the Pd_{31} cluster was established to simulate the edge and plane sites. The results indicated that H_2O_2 could be readily generated on more saturated sites, while it is easier to decompose on more coordinatively unsaturated sites. Thus, it can be seen that different active sites have various activity and selectivity owing to atomic arrangements.[47] Similarly, the single-crystal Pd(100) was found to be far more active than the corresponding polycrystalline surface,[48] followed by Xia and co-workers,[49] suggesting that H_2O_2 is more prone to decompose on Pd(111) than that on Pd(100). Currently, most theoretical works on DSHP are limited to the active site, with few exploratory studies focused on the Pd nanoparticles. In our previous work,[50] we designed a polyhedral nanoparticle catalyst through theoretical calculations. The relationship between size and selectivity was studied from the perspective of active sites.[51−54] Despite tremendous efforts devoted to the active sites, precise information concerning the catalytic sites governing the direct synthesis of H_2O_2 on Pd nanoparticles has not yet been achieved yet.

In addition, a gap exists between the catalysts used in experiments and theoretical simulations. To a large extent, this gap can be attributed to dynamic structural changes[55−57] in the nanoparticle during the heterogeneous catalytic reaction, resulting in significant debates on active centers.[58,59] Notably, the coverage of the coadsorbed species varies widely with reaction conditions, which would cause dynamic structural changes, exhibiting quite a different influence on the activity and selectivity due to different oxidation states of the catalyst. Selinsek et al.[59] observed that the oxidation state and local Pd structure vary with the reactant ratio (H_2/O_2), leading to a difference in the yield of H_2O_2. Xu et al. indicated that the selectivity of H_2O_2 can be enhanced by coadsorbed O.[60] This phenomenon demonstrated that surface states vary with ambient reactive gases (H_2 and O_2) and coadsorbed species, which could affect the reaction mechanism.[56,61,62] Wilson and co-workers[28] believed that differences in turnover rates and selectivity between Pd clusters of different sizes result from changes in the stability of surface intermediates and transition states. In most computational studies, the focus is primarily on active site descriptions[62−64] while neglecting the influence of nanoparticle size and environmental effects (temperature, pressure, and coverage). An advanced coverage-dependent kinetic model combined with the energetics from first-principles calculations was developed recently, providing a significant advance in understanding the reaction mechanism of heterogeneous catalysis.[62−65] Our previous work showed that the adsorbate−adsorbate interactions considerably affect the reaction mechanism of the synthesis of hydrogen peroxide on Pd(111).[62] Undeniably, the elusive reaction mechanism issues are always present because the coverages of species on various sizes of Pd nanoparticles change dynamically. Therefore, a method combined with size-dependent and coverage-dependent modeling should be developed to analyze reaction mechanisms on nanoparticles quantitatively.

In this work, to describe the relationship between the Pd particle size and active sites, we chose Pd(111) as the closely arranged planar site in nanoparticles, Pd(100) as the loosely organized planar site, and Pd(211) as the step site. The Pd_{13} cluster was selected to represent the corner site. To approach more realistic conditions, a microkinetic model was developed with size-dependent and coverage effects to study the mechanism of the direct synthesis of hydrogen peroxide on Pd nanoparticles. We aim to answer the following major questions: (i) What are the mechanisms of direct synthesis of H_2O_2 reaction on Pd nanoparticles with lateral interactions? (ii) How do temperature and H_2/O_2 partial pressure affect the selectivity and activity of the reaction on the Pd nanoparticles with different sizes? (iii) How can we understand the origin of size effects?

2. MODEL AND COMPUTATIONAL METHODS

2.1. Surface Model. Pd nanoparticles are typical active centers for the direct synthesis of hydrogen peroxide and can be classified into three types of sites (terrace, step, and corner).[13,43,50] In this work, we assumed the Pd nanoparticles used in the experiments were all in the same cuboctahedral shape of various sizes (Figure S3). Three surfaces ((Pd(111), Pd(211), and Pd(100)) and a Pd_{13} cluster were utilized to simulate the active sites on the Pd nanoparticles. Pd(111) and Pd(100) represent various terrace sites with the lowest surface energies among the clean Pd facets, which are the most abundant in large nanoparticles. Pd(211) denotes step sites, which consist of Pd(111) and Pd(100). Pd_{13} cluster represents the corner sites.

2.2. Computational Methods. Density functional theory (DFT) simulations in this work were conducted for the direct synthesis of hydrogen peroxide within the framework of the generalized gradient approximation (GGA) based on Perdew−Burke−Ernzerhof[66] (PBE) functional using the VASP code.[67,68] All initial states, transition states, and final states were computed by the DFT-D3 method,[69−73] considering the van der Waals interaction.[64,74,75] The project-augmented wave (PAW)[76,77] was carried out to describe the interaction between core electrons and valence electrons. A plane-wave basis set was

https://doi.org/10.1021/acscatal.3c03893
ACS Catal. 2023, 13, 15054−15073

Scheme 1. Flow Chart of Iteration Process for the Coverage-Dependent Microkinetic Model. X Represents the Error of Each Species Coverage on the Entire Analytical Procedure and Is Less than 0.01 ML

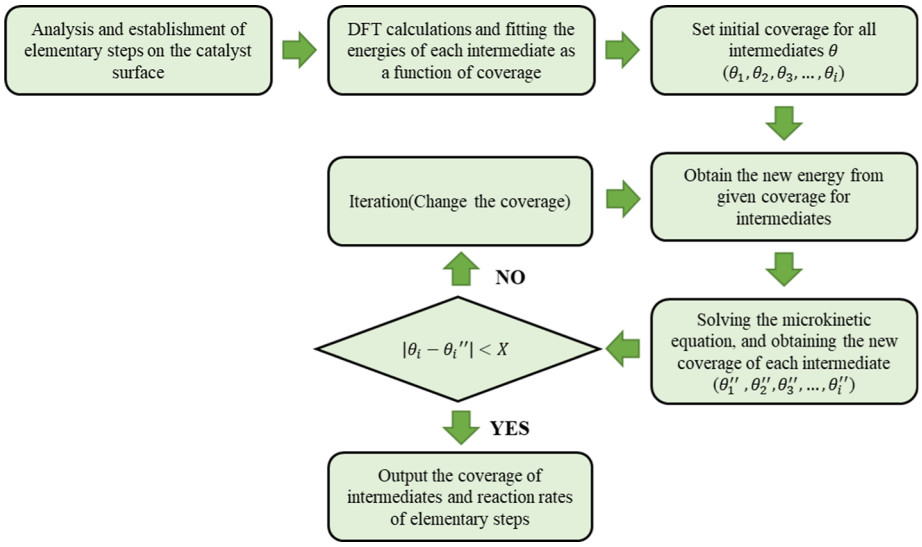

expanded with a kinetic cutoff energy of 400 eV. The Pd(100), Pd(111), and Pd(211) surfaces were modeled using a slab geometry with a periodically repeated (3 × 3) unit cell, and PdO(101)[59,78−80] was used as a (4 × 2) unit cell. (3 × 3 × 1) Monkhorst−Pack *k*-point mesh sampling[81] was employed for Pd(100) and Pd(111), and (4 × 3 × 1) Monkhorst−Pack *k*-point mesh was used for Pd(211) and PdO(101). For the Pd_{13} cluster, (1 × 1 × 1) Monkhorst−Pack *k*-point mesh was utilized. Structure optimization was conducted using the conjugate-gradient algorithm with electronic convergence of 10^{-5} eV and geometric convergence of 0.01 eV/Å. The transition states (TSs) were searched using the method called a constrained optimization scheme,[82−84] confirmed by two rules: (i) the forces of atoms should be optimized to be less than 0.01 eV/Å and (ii) there should be a maximum energy along the reaction coordinate, but a minimum energy on all other degrees of freedom. All optimized initial states, transition states, and final states were verified by frequency analysis[85] using a finite displacement method to the mass-weighted Hessian matrix. The free-energy corrections for molecules in the gas phase were calculated using the Gaussian 09 package,[86] and the basis set was B3LYP/6-311+G*.[87,88]

2.3. Choice of Elementary Steps. To gain insight into the direct synthesis of hydrogen peroxide,[62] all possible reaction pathways corresponding to the formation of H_2O_2 and H_2O, including the decomposition of H_2O_2, were investigated on Pd(100), Pd(111), and Pd(211). The complete elementary steps were performed as follows: (1) O_2 adsorption (R1: $O_2 + * \rightleftarrows O_2*$); (2) H_2 dissociation (R2: $H_2 + * + * \rightleftarrows H* + H*$); (3) O_2 dissociation (R3: $O_2* + * \rightleftarrows O* + O*$); (4) O_2 hydrogenation to OOH (R4: $O_2* + H* \rightleftarrows OOH* + *$); (5) hydrogenation of OOH to H_2O_2 (R5: $OOH* + H* \rightleftarrows H_2O_2 + * + *$); (6) OOH dissociation (R6: $OOH* + * \rightleftarrows O* + OH*$); (7) hydrogenation of O to OH (R7: $O* + H* \rightleftarrows OH* + *$); (8) OH hydrogenation to H_2O (R8: $OH* + H* \rightleftarrows H_2O + * + *$); (9) 2OH synthesis to H_2O and O (R9: $OH* + OH* \rightleftarrows H_2O + * + O*$); and (10) H_2O_2 decomposition to two OH (R10: $OH* + OH* \rightleftarrows H_2O_2 * + *$).

The key intermediate in the direct synthesis of hydrogen peroxide should be noted. In addition to the above-mentioned hydrogenation of O_2 ($O_2* + H* \rightleftarrows OOH* + *$), there are some papers[89,90] in the literature, showing that the formation of OOH takes place by proton transfer from water ($O_2* + H_2O + * \rightleftarrows OOH* + OH*$). Inspired by the work of Greeley and Rankin,[90] we investigated both OOH formation mechanisms with coverage effects on Pd(100) (dominated active sites on Pd nanoparticles). First, the reaction of $O_2* + H_2O + * \rightleftarrows OOH* + OH*$ on Pd(100) was investigated from a low temperature (273.15 K) to a high temperature (323.15 K) (Figures S131−133). Our findings revealed that this reaction pathway does not significantly contribute to the formation of OOH* but primarily represents the reverse reaction pathway, leading to water and oxygen production. The reaction rate for $OOH* + OH* \rightarrow O_2* + H_2O + *$ is considerably lower than that of $OH* + H* \rightarrow H_2O + * + *$, and therefore, it does not serve as the primary route for water formation. Subsequently, we compared the mechanisms of direct hydrogen peroxide synthesis with and without the involvement of $O_2* + H_2O + * \rightleftarrows OOH* + OH*$. It was observed that the primary reaction mechanisms on the Pd(100) surface are the same under both mechanisms ($O_2* + H* \rightarrow OOH* + *$, and $O_2* + H_2O + * \rightleftarrows OOH* + OH*$). Furthermore, we conducted a comparative analysis of surface coverage, activity, and selectivity. There were no significant changes in coverage, activity, and selectivity with and without $O_2* + H_2O + * \rightleftarrows OOH* + OH*$. Hence, $O_2* + H_2O + * \rightleftarrows OOH* + OH*$ is not a crucial step in generating OOH*, nor is it a significant step for H_2O formation. Therefore, we do not consider $O_2* + H_2O + * \rightleftarrows OOH* + OH*$ further in this work.

2.4. Microkinetic Model. A microkinetic model with a coverage effect was performed to study the mechanism of the direct synthesis of hydrogen peroxide. The rate constants of each elementary step were determined using transition states theory. The equation is as follows

$$k_i = \frac{k_B T}{h} e^{-\Delta G_i^{\neq 0}/k_B T} \quad (1)$$

where k_B is the Boltzmann constant, T is the temperature, h is the Planck's constant, and $\Delta G_i^{\neq 0}$ is the change of standard molar Gibbs free energies between the transition state and the initial state for step i from DFT calculations. More details of the calculation are provided in the Supporting Information.

https://doi.org/10.1021/acscatal.3c03893
ACS Catal. 2023, 13, 15054−15073

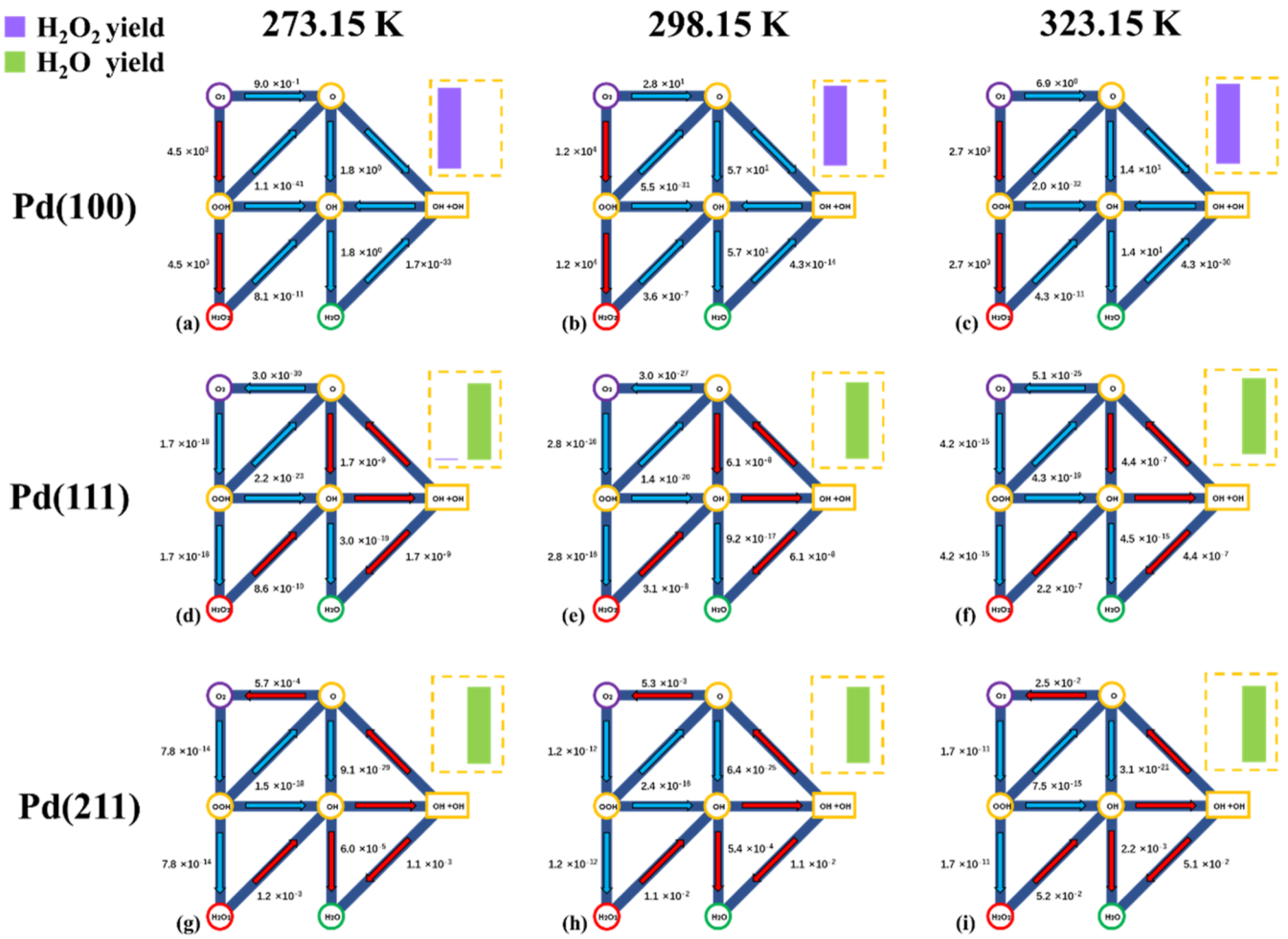

Figure 1. Coverage-dependent reaction pathways for the production of H_2O_2 and H_2O on (a–c) Pd(100), (d–f) Pd(111), and (g–i) Pd(211). The red arrow is the major pathway according to the results of the coverage-dependent microkinetic model. The values are the reaction rates (units are s^{-1}) for each elementary step. The green column represents the yield of H_2O, and the purple column represents the yield of H_2O_2. The reaction conditions are $P_{O_2} = P_{H_2} = 0.5$ bar, $P_{H_2O_2} = P_{H_2O} = 0.035$ bar, and $T = 273.15$, 298.15, and 323.15 K.

The coverage-dependent microkinetic models[63,64,91] based on first-principles calculations have achieved significant progress in the study of heterogeneous catalytic reactions with both self-interactions and cross-interactions. The low coverage range is defined when all of the first neighbor sites for each adsorbate are free. In the high-coverage region, the effect of adsorbate–adsorbate interactions exhibits a significant increase with more adsorbed species on the surface. The differential generalized formation energy[63,92,93] for multiple adsorbates as a function of coverage takes the following equation

$$E_i(\theta) = f(\theta_{i0}) + \sum_j f_{i/j}(\theta_{\text{total}}) - f(\theta_{i0})\frac{\theta_j}{\theta_{\text{total}}} \quad (2)$$

where $E_i(\theta)$ represents the differential generalized formation energy of adsorbate i at the specific coverage θ, $f(\theta_{i0})$ is the differential generalized formation energy at low coverage, and $f_{i/j}(\theta_{\text{total}})$ is the differential generalized formation energy of adsorbate i under the environment of j at the coverage of θ_{total}, i and j can be the same species. More details are provided in the Supporting Information.

The core concept of coverage-dependent microkinetic modeling is shown in Scheme 1. In this model, the abundance of each species eventually converges to a sufficient extent, and the error of each species that converges on the entire analytical procedure is less than 0.01 ML.

2.5. Surface Phase Diagram Calculation Method. Determine the stability of the system under consideration by building phase diagrams[80,94–99] of the surfaces in contact with the gas environment (H_2 and O_2). The adsorption stability of H_2 and O_2 on Pd(100) was determined by comparing the Gibbs free energies of adsorption (ΔG^{ads}). ΔG^{ads} was obtained relative to the clean surfaces of Pd(100) and evaluated as a function of $H_2(\mu_{H2})$ and $O_2(\mu_{O2})$ chemical potentials.

$$\Delta G^{\text{ads}} = \frac{1}{2A}\left[G^{\text{surf}}_{i/\text{Pd}(100)} - G^{\text{surf}}_{\text{Pd}(100)} - \frac{N_O}{2}\mu_{O_2} - \frac{N_H}{2}\mu_{H_2}\right] \quad (3)$$

where A is the surface area, $G_{i/\text{Pd}(100)}{}^{\text{surf}}$ is the Gibbs free energy of adsorption of intermediate on the Pd(100), and i is the species of intermediates. $G_{\text{Pd}(100)}{}^{\text{surf}}$ is the Gibbs free energy on the clean surfaces of Pd(100). μ_i is the chemical potentials of various species i and dependent on temperature and pressure; the equation is as follows

$$\mu_x(T, P_x) = E_x + \Delta\mu_x(T, P^0) + k_B T \ln\left(\frac{P_x}{P^0}\right) \quad (4)$$

https://doi.org/10.1021/acscatal.3c03893
ACS Catal. 2023, 13, 15054–15073

where x is H_2 or O_2, P^0 is the standard pressure, and $\Delta\mu_x(T, P^0)$ is the chemical potential at the standard pressure. The stable structure under a given condition (T, P_{H_2}, and P_{O_2}) is obtained by the structure that minimizes ΔG^{ads}.

Under hydrogen-lean and oxygen-rich conditions, an extended palladium oxide bulk is thermodynamically stable, which gives

$$\mu_{PdO}^{bulk} < \mu_{Pd}^{bulk} + \frac{1}{2}\mu_{O_2} \quad (5)$$

whereas under oxygen-lean and hydrogen-rich conditions, PdH is thermodynamically stable, which gives

$$\mu_{PdH}^{bulk} < \mu_{Pd}^{bulk} + \frac{1}{2}\mu_{H_2} \quad (6)$$

Under balanced conditions, the coverage-dependent surface is thermodynamically stable, which gives

$$\begin{aligned}\mu_{PdX} &< \mu_{Pd}^{bulk} + \frac{n}{2}\mu_{O_2} + \frac{m}{2}\mu_{H_2},\ \mu_{PdX} + \frac{1-n}{2}\mu_{O_2} \\ &< \mu_{PdO}^{bulk} + \frac{m}{2}\mu_{H_2},\ \text{and}\ \mu_{PdX} + \frac{1-m}{2}\mu_{H_2} \\ &< \mu_{PdH}^{bulk} + \frac{n}{2}\mu_{O_2} \end{aligned} \quad (7)$$

where PdX denotes a slab with coverage of species, and n and m represent the contents of H and O in PdX.

3. RESULTS AND DISCUSSION

3.1. Size-Dependent Microkinetic Modeling. The size-dependent microkinetic modeling incorporating coverage effects was developed and applied in this work. Typically, Pd nanoparticles consist of three kinds of reaction sites (terrace, step, and corner).[41,42,50] In this work, we disregarded corner sites based on the following reasons: (i) the proportion of corner sites on Pd nanoparticles ranging from 2 to 30 nm is extremely low, as illustrated in Figure S3b,c. (ii) According to the coverage-dependent microkinetic model, the main species on the Pd_{13} cluster is O (99.9%), rendering the corner sites entirely poisoned. (iii) H_2O is the primary product on the Pd_{13} cluster, and its activity is considerably inferior (approximately 10^{-15} s^{-1}) compared to Pd(100), Pd(111), and Pd(211) surfaces. (iv) The pressure does not have a major effect on selectivity of Pd_{13} cluster for the direct synthesis of H_2O_2. (v) Temperature has a great influence on the activity of the Pd_{13} cluster, but the activity is always lower than the other three surfaces, as depicted in Figure S3d–l. The cuboctahedral nanoparticle model was utilized to represent the relationship between size and proportion of active sites (Table S2). The proportion of terrace sites ((Pd(111), Pd(100)) increases with a rise in the size of nanoparticles, whereas the proportion of edge sites ((Pd(211)) exhibits an opposite trend.

3.2. Detailed Comparison of the Mechanism of H_2O_2 and H_2O Formation on Three Surfaces (Pd(100), Pd(111), Pd(211)) on Pd Nanoparticles. *3.2.1. Pathway Comparison on the Three Surfaces from Low Temperature to High Temperature.* The mechanism for the direct synthesis of hydrogen peroxide involves the main reactions (synthesis of H_2O_2) and side reactions (formation of H_2O), leading to the whole process being much more complex. Notably, the dissociation of H_2O_2 to two OH species is an important elementary step for H_2O formation, and it is one of the significant factors leading to a low hydrogen peroxide yield. It is revealed that H_2O_2 decomposition is more likely to occur on coordinatively unsaturated sites, such as corner sites or edge sites.[25] In this work, three typical temperatures were considered in our simulations, namely, low temperature (273.15 K), moderate temperature (298.15 K), and high temperature (323.15 K). The entire mechanism for the direct synthesis of hydrogen peroxide can be divided into three kinds of pathways: (i) the synthesis of H_2O_2; (ii) the decomposition of H_2O_2; and (iii) the formation of H_2O, as shown in Figure 1.

3.2.1.1. Synthesis of H_2O_2. We first simulated the synthesis of H_2O_2 on the three surfaces (Pd(100), Pd(111), and Pd(211)), and reaction pathways were summarized as follows: (i) $H_2 + * + * \rightarrow H^* + H^*$; (ii) $O_2 + * \rightarrow O_2^*$; (iii) $O_2^* + H^* \rightarrow OOH^* + *$; (iv) $OOH^* + H^* \rightarrow H_2O_2 + * + *$. After carefully comparing the reaction channels among Pd(100), Pd(111), and Pd(211) at moderate temperature (298.15 K), we found that the rate-determining steps are the O_2 hydrogenation on Pd(100) (E_a = 0.46 eV) (Table S7) and H_2 dissociation on Pd(211) (E_a = 0.88 eV) (Table S13), while the rate-determining step on Pd(111) is the OOH hydrogenation (E_a = 1.14 eV) (Table S19). The reaction rate of H_2O_2 increases from low temperature (10^3 s^{-1}) to moderate temperature (10^4 s^{-1}) on Pd(100), followed by the yield of H_2O_2 decreasing dramatically from moderate temperature (10^4 s^{-1}) to high temperature (10^3 s^{-1}). Our results indicate that the peak of the H_2O_2 formation is around moderate temperature as displayed in Figure S106. As for Pd(111) and Pd(211), the yield of H_2O_2 continuously increases from low temperature to high temperature. Additionally, the yield of H_2O_2 is in the order of Pd(100) > Pd(211) > Pd(111), indicating that Pd(100) contains the dominant active sites for the synthesis of H_2O_2.

3.2.1.2. Decomposition of H_2O_2. With respect to the second part of the mechanism, the decomposition of H_2O_2 ($H_2O_2 + * + * \rightarrow OH^* + OH^*$) was considered. The barrier of HO−OH bond breaking on the three surfaces is in the order of Pd(111) (1.05 eV) > Pd(100) (1.00 eV) > Pd(211) (0.72 eV) at moderate temperature. The decomposition rate of hydrogen peroxide on Pd(100) reaches the maximum value from low temperature to moderate temperature, followed by a dramatic decline. It is interesting to note that the rate of H_2O_2 decomposition on Pd(100) is higher than that on Pd(111) at moderate temperature, while the opposite trend is observed at low and high temperatures. In addition, the rate of H_2O_2 decomposition on Pd(211) is highest compared to that on Pd(100) and Pd(111), making it the dominant active site for HO−OH bond breaking.

3.2.1.3. Formation of H_2O. The mechanism of H_2O formation can be divided into two parts. The first part is the OH* formation, and the second is the conversion of OH* to H_2O. The formation of OH* comes from three channels: (i) $H_2 + * + * \rightarrow H^* + H^*$, $O_2^* + * \rightarrow O^* + O^*$, $O^* + H^* \rightarrow OH^* + *$; (ii) $H_2 + * + * \rightarrow H^* + H^*$, $O_2 + * \rightarrow O_2^*$, $O_2^* + H^* \rightarrow OOH^* + *$, $OOH^* + * \rightarrow O^* + OH^*$; and (iii) $H_2 + * + * \rightarrow H^* + H^*$, $O_2 + * \rightarrow O_2^*$, $O_2^* + H^* \rightarrow OOH^* + *$, $OOH^* + H^* \rightarrow H_2O_2 + * + *$, $H_2O_2 + * + * \rightarrow OH^* + OH^*$. On Pd(100), the rate-determining step of channel (i) is $O_2^* + * \rightarrow O^* + O^*$ (E_a = 0.61 eV, 298.15 K), channel (ii) is $OOH^* + * \rightarrow O^* + OH^*$ (E_a = 2.35 eV, 298.15 K), and channel (iii) is $H_2O_2 + * + * \rightarrow OH^* + OH^*$ (E_a = 1.00 eV, 298.15 K). Compared to the barriers of the three channels, the formation of OH* mainly comes from channel (i). Additionally, channel (iii) is more likely to occur than the other two channels on Pd(111) and Pd(211).

https://doi.org/10.1021/acscatal.3c03893
ACS Catal. 2023, 13, 15054−15073

(a)

Elementary Steps	Pd(100)			Pd(111)			Pd(211)		
	273.15 K	298.15 K	323.15 K	273.15 K	298.15 K	323.15 K	273.15 K	298.15 K	323.15 K
O_2+* ⇋ O_2*	0.00	0.00	0.00	0.00	0.00	0.00	0.00	0.00	0.00
H_2+*+* ⇋ H*+H*	0.00	0.00	0.00	0.00	0.00	0.00	1.09	1.15	1.10
O_2*+* ⇋ O*+O*	0.00	0.00	-0.03	0.00	0.00	0.00	0.60	0.59	0.60
O_2*+H* ⇋ OOH*+*	0.98	0.99	0.62	0.99	0.99	0.98	0.94	0.88	0.93
OOH*+H* ⇋ H_2O_2+*+*	0.02	0.01	0.38	0.01	0.01	0.02	0.06	0.12	0.07
OOH*+* ⇋ O*+OH*	0.00	0.00	0.00	0.00	0.00	0.00	0.00	0.00	0.00
O*+H* ⇋ OH*+*	0.00	0.00	0.03	1.35	1.30	1.27	0.00	0.00	0.00
OH*+H* ⇋ H_2O+*+*	0.00	0.00	0.00	0.00	0.00	0.00	-1.06	-1.12	-1.07
OH*+OH* ⇋ H_2O+O*+*	0.00	0.00	0.00	0.00	0.00	0.00	0.68	0.70	0.67
OH*+OH* ⇋ H_2O_2+*+*	0.00	0.00	0.00	-1.35	-1.30	-1.27	-1.31	-1.33	-1.29

(b)

Elementary Steps	Pd(100)			Pd(111)			Pd(211)		
	273.15 K	298.15 K	323.15 K	273.15 K	298.15 K	323.15 K	273.15 K	298.15 K	323.15 K
O_2+* ⇋ O_2*	0.00	0.00	0.00	0.00	0.00	0.00	0.00	0.00	0.00
H_2+*+* ⇋ H*+H*	0.00	0.00	0.00	0.00	0.00	0.00	1.02	1.02	1.02
O_2*+* ⇋ O*+O*	1.00	1.00	0.97	0.00	0.00	0.00	0.60	0.59	0.60
O_2*+H* ⇋ OOH*+*	-0.01	0.00	-0.04	0.00	0.00	0.00	0.00	0.00	0.00
OOH*+H* ⇋ H_2O_2+*+*	0.01	0.00	0.04	0.00	0.00	0.00	0.00	0.00	0.00
OOH*+* ⇋ O*+OH*	0.00	0.00	0.00	0.00	0.00	0.00	0.00	0.00	0.00
O*+H* ⇋ OH*+*	0.00	0.00	0.03	0.85	0.81	0.78	0.00	0.00	0.00
OH*+H* ⇋ H_2O+*+*	0.00	0.00	0.00	1.00	1.00	1.00	0.00	0.00	0.00
OH*+OH* ⇋ H_2O+O*+*	0.00	0.00	0.00	0.00	0.00	-0.01	0.15	0.14	0.13
OH*+OH* ⇋ H_2O_2+*+*	0.00	0.00	0.00	-0.85	-0.80	-0.78	-0.77	-0.75	-0.74

(c)

Elementary Steps	Pd(100)			Pd(111)			Pd(211)		
	273.15 K	298.15 K	323.15 K	273.15 K	298.15 K	323.15 K	273.15 K	298.15 K	323.15 K
O_2+* ⇋ O_2*	0.00	0.00	0.00	0.00	0.00	0.00	0.00	0.00	0.00
H_2+*+* ⇋ H*+H*	0.00	0.00	0.00	0.00	0.00	0.00	0.02	0.02	0.02
O_2*+* ⇋ O*+O*	0.00	0.00	-0.03	0.00	0.00	0.00	0.60	0.59	0.60
O_2*+H* ⇋ OOH*+*	-0.01	0.00	-0.04	0.00	0.00	0.00	0.00	0.00	0.00
OOH*+H* ⇋ H_2O_2+*+*	0.01	0.00	0.04	0.00	0.00	0.00	0.00	0.00	0.00
OOH*+* ⇋ O*+OH*	0.00	0.00	0.00	0.00	0.00	0.00	0.00	0.00	0.00
O*+H* ⇋ OH*+*	0.00	0.00	0.03	1.35	1.30	1.27	0.00	0.00	0.00
OH*+H* ⇋ H_2O+*+*	0.00	0.00	0.00	0.00	0.00	0.00	0.00	0.00	0.00
OH*+OH* ⇋ H_2O+O*+*	0.00	0.00	0.00	0.00	0.00	0.00	0.15	0.14	0.13
OH*+OH* ⇋ H_2O_2+*+*	1.00	1.00	1.00	-0.35	-0.30	-0.27	0.24	0.25	0.26

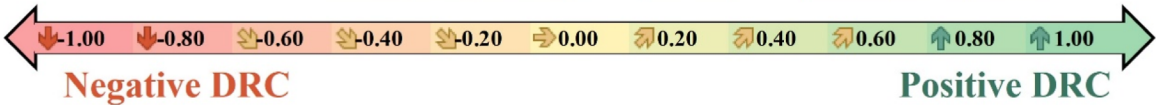

Figure 2. Degrees of rate control from the elementary steps on (a) OOH * + H * ⇄ H_2O_2 + * + *; (b) those on OH * + H *⇄ H_2O + * + *; and (c) those on OH* + OH* ⇄ H_2O_2+ * + * on Pd(100), Pd(111), and Pd(211).

Regarding the conversion of OH* to H_2O, there are two elementary steps, namely, (i) OH* + H* → H_2O + * + * and (ii) OH* + OH* → H_2O + O* + *. It is found that step ii is more prone to occur than step (i) on Pd(111) and Pd(211), while the opposite phenomenon appears on Pd(100).

The major pathway for H_2O formation on Pd(100) can be summarized as follows: H_2 + * + * → H* + H*, O_2* + * → O* + O*, O* + H* → OH*, OH* + H* → H_2O + * + *. With respect to Pd(111) and Pd(211), H_2O formation is more likely to occur in the other channel, namely, H_2 + * + * → H* + H*, O_2 + * → O_2*, O_2* + H* → OOH* + *, OOH* + H* → H_2O_2 + * + *, H_2O_2 + * + * → OH* + OH*, and OH* + OH* → H_2O + O* + *. Compared to the rate-determining step for H_2O formation, the barrier is in the order Pd(111) (H_2O_2 + * + * → OH* + OH*, E_a = 1.05 eV) > Pd(211) (H_2 + * + * → H* + H*, E_a = 0.88 eV) > Pd(100) (O_2* + * → O* + O*, E_a = 0.61 eV).

Overall, for selectivity, H_2O_2 is the main product on Pd(100), while H_2O is more likely to occur on Pd(111) and Pd(211). Significantly, the reaction rates of H_2O_2 and H_2O on Pd(100) are much higher than those on the other two surfaces, making it the dominant active site on Pd nanoparticles. Furthermore, the optimized temperature for the direct synthesis of H_2O_2 on Pd(100) is located at the moderate temperature. The yields of H_2O_2 and H_2O increase continuously from low temperature to high temperature on Pd(111) and Pd(211) (Figure S106).

3.2.2. Analysis of the Degree of Rate Controls on the Three Surfaces from Low Temperature to High Temperature. In order to quantitatively determine the significant steps that control the rates of H_2O and H_2O_2 formation on Pd(100), Pd(111) and Pd(211) from low temperature to high temperature, the concept of rate control degree proposed by Campbell et al.[100−103] was utilized, and the equation is shown as follows

$$X_{\mathrm{DRC},i} = \frac{k_i}{r}\left(\frac{\partial r}{\partial k_i}\right)_{k_{j\neq i}, K_i} = \left(\frac{\partial \ln r}{\partial \ln k_i}\right)_{k_{j\neq i}, K_i} \quad (8)$$

https://doi.org/10.1021/acscatal.3c03893
ACS Catal. 2023, 13, 15054−15073

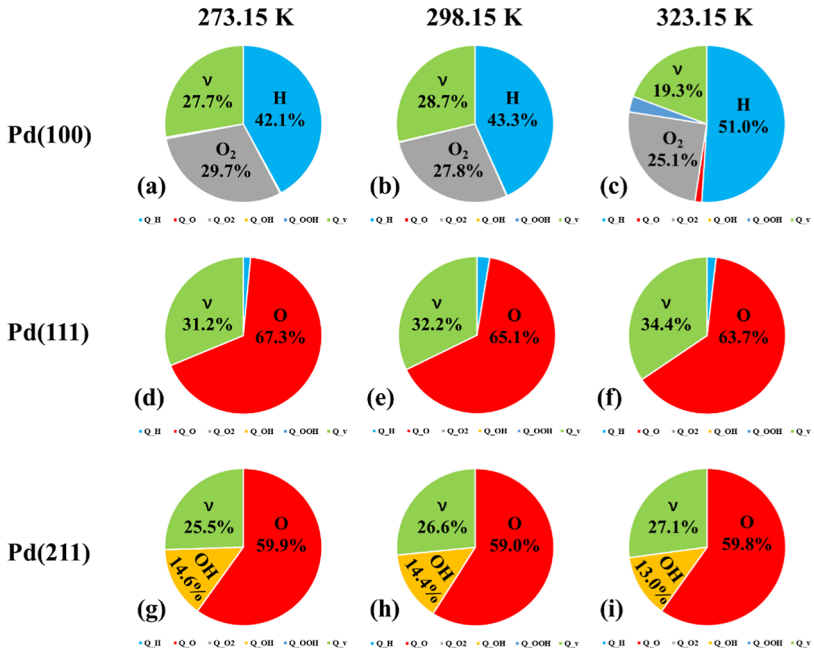

Figure 3. Ratios of main species coverage analyses from 273.15 to 323.15 K on (a–c) Pd(100), (d–f) Pd(111), and (g–i) Pd(211). The red is O, blue is H, green is free sites, gray is O_2, and yellow is OH ($P_{O_2} = P_{H_2} = 0.5$ bar and $P_{H_2O_2} = P_{H_2O} = 0.035$ bar).

where $X_{DRC,j}$ is the DRC value of elementary reaction step i for the production of H_2O or H_2O_2, r is the formation rate of H_2O or H_2O_2, k_i is the forward rate constant of elementary step i, and K_i is equilibrium constant for elementary step *i*. The larger the $|X_{DRC,i}|$ value, the larger its influence is on the production rate of water or hydrogen peroxide. A positive DRC value represents that it would inhibit the overall reaction rate r, if we increased the barrier of elementary step *i*. Similarly, a negative value of DRC leads to the contrary effect.

Three important elementary steps were investigated through the detailed analysis of the degree of rate control (Figure 2) at different temperatures, namely, (i) OOH* + H * ⇄ H_2O_2 + * + *; (ii) OH * + H * ⇄ H_2O + * + *; and (iii) OH* + OH* ⇄ H_2O_2 + * + *.

3.2.2.1. DRC Analysis of (i) OOH + H * ⇄ H_2O_2 + * + *.* First, we focused on the DRC values of step (i), which is the essential step for H_2O_2 formation. Notably, Pd(100) is the significant surface for the formation of H_2O_2 according to our simulation. Thus, OOH * + H * → H_2O_2 + * + * on Pd(100) was analyzed in detail (Figure 2a). Step (i) is mainly controlled by the step of O_2* + H * → OOH* + * from low to high temperature, and its DRC values are 0.98 (low temperature), 0.99 (moderate temperature), and 0.62 (high temperature). Therefore, lowering the barrier of O_2 hydrogenation is beneficial to the reaction of OOH hydrogenation; a higher O_2 hydrogenation barrier will reduce the abundance of OOH species, which inhibits the conversion of OOH to H_2O_2. Additionally, when the temperature increases from low temperature to moderate temperature, the value of DRC changes slowly. However, in the range of 298.15 K < *T* < 323.15 K, the value of DRC (O_2* + H * → OOH* + *) decreases from 0.99 to 0.62. It is worth mentioning that the value of DRC (OOH * + H * → H_2O_2 + * + *) enhances from 0.01 to 0.38, and the lower barrier of OOH * + H * → H_2O_2 + * + * promotes the formation of H_2O_2. Significantly, the difference between the DRC value of O_2* + H * → OOH* + * and that of OOH * + H * → H_2O_2 + * + * is 0.24 at the high temperature. It indicates that decreasing the barrier of O_2* + H * → OOH* + * is more effective than lowering the energy barrier of O_2* + * → O* + O*. More details of DRC analysis on Pd(111) and Pd(211) are provided in the Supporting Information.

*3.2.2.2. DRC Analysis of (ii) OH * + H * ⇄ H_2O + * + *.* Upon reviewing the reaction pathways with the coverage effects, we found that the reaction OH* + H* → H_2O + * + * is the major pathway for the formation of H_2O on Pd(100) (Figure 2b). It is mainly controlled by the step of O_2* + * → O* + O* from low temperature to high temperature, and the DRC values are 1.00 (low temperature), 1.00 (moderate temperature), and 0.97 (high temperature), respectively. Lowering the barrier for O−O bond breaking can enrich the O species, which facilitates O conversion to OH and ultimately accelerates the OH hydrogenation process.

3.2.2.3. DRC Analysis of (iii) OH + OH* ⇄ H_2O_2 + * + *.* For the formation of H_2O, the reaction H_2O_2 + * + * → OH* + OH* is the major pathway for Pd(111) and Pd(211). It can be seen that O* + H* → OH* + * makes the major contribution to H_2O_2 + * + * → OH* + OH* on Pd(111) (Figure 2c). The DRC values of O hydrogenation decrease slightly (from 1.35 to 1.27) with the increase in temperature (from low-to high temperature). Decreasing the energy barrier of O* + H* → OH* + * can enhance the concentration of free sites and OH species, and abundant free sites facilitate the decomposition of H_2O_2. It is also found that the increase in coverage of OH species can accelerate two OH conversions to H_2O, which will consume more OH, thereby promoting the rate of H_2O_2 + * + * → OH* + OH*. On Pd(211), the reaction H_2O_2 + * + * → OH* + OH* is affected by three steps, and the DRC values are in the order of O* + O* → O_2* + * > H_2O_2 + * + * → OH* + OH* > OH* + OH* → H_2O + O* + *. The O_2 formation is a dominant step, and the DRC value is around 0.60 from low temperature to high temperature. Lowering the barrier of O* + O* → O_2* + * can enrich the abundance of free sites and O_2. For H_2O_2 formation, O_2 is the critical intermediate that is favored to generate OOH, thereby accelerating the production of hydrogen peroxide. High

https://doi.org/10.1021/acscatal.3c03893
ACS Catal. 2023, 13, 15054−15073

concentrations of free sites can accelerate the decomposition of H_2O_2.

3.2.3. Coverage Comparison on the Three Surfaces and State Analysis. 3.2.3.1. Coverage Comparison on the Three Surfaces from Low Temperature to High Temperature. To provide insight into the changes of intermediates on the different surfaces and the influence of temperature on coverage, coverage-dependent kinetic modeling analysis was carried out from low temperature to high temperature. It shows that the coverage of intermediates varies significantly with the change of active sites (Figure 3). Several striking features are revealed in our simulations. First, the surface of Pd(100) is mainly occupied by O_2 (29.7%), H (42.1%) and free sites (27.7%) at the low temperature. The coverage of O_2 decreases slightly from 29.7 to 25.1% from low temperature to high temperature, while the coverage of H increases gradually from 42.1 to 51.0%. It is interesting to note that the coverage of free sites improves marginally from 27.7 to 28.7% in the range of 273.15 K < T < 298.15 K, followed by a considerable decline from 28.7% to 19.3% (298.15 K < T < 323.15 K). At high temperature, OOH and O also occupy a certain proportion of the surface besides O_2, H, and free sites. Second, the main species on Pd(111) are O (67.3%), H (1.5%), and free sites (31.2%) at low temperature. This result indicates that the Pd(111) surface is almost completely occupied by O and free sites, when H_2O_2 decomposition is considered in the current simulation. As the temperature rises, the coverage of O decreases, while the coverage of the free site follows the opposite trend. Third, the surface of Pd(211) is mainly occupied by the O, OH, and free sites. The proportion of OH decreases slightly with temperature increase, while free sites show the contrary tendency.

Notably, the major species on Pd(100) are different from those on Pd(111) and Pd(211), resulting in various products. O_2 and H are the main species on Pd(100), which are beneficial to the elementary step of O_2* + H* → OOH* + *, further promoting the following OOH hydrogenation. On Pd(111), the main coverages are those of the O and free sites. High concentrations of free sites facilitate the dissociation of O_2, OOH, and H_2O_2. Meanwhile, the lack of H species is unfavorable for the hydrogenation of O_2 to generate OOH, resulting in the inhibition of the production of hydrogen peroxide. The coverage of OH on the Pd(211) surface is around 14%, which is different from that on Pd(111), accelerating the process of OH* + OH* → H_2O + O* + *, making the rate of H_2O formation on Pd(211) higher than that on Pd(111).

3.2.3.2. State Analysis of Pd(100). Based on our simulations, Pd(100) is the most significant surface for H_2O_2 formation with high activity and selectivity, larger than those on Pd(111) and Pd(211). Pd(100) is exposed to reactants (H_2 and O_2) in the direct synthesis of H_2O_2, suggesting that it is important to investigate it in a gas mixture environment. In this work, we employed a specialized, constrained equilibrium approach.[95,104] This methodology assumes that the surface is in complete thermodynamic equilibrium with separate gas-phase reservoirs of O_2 and H_2, while preventing any possibility of a reaction between the surface of O_2 and H_2. In the case of lower chemical potentials of H_2 and O_2, the clean surface of Pd(100) is the stable phase (Figure 4). If the H_2 chemical potential is kept low and the O_2 chemical potential increases (along the y-axis) to oxygen-rich conditions, first O_2 covers the Pd(100) surface, and then the PdO(101) phase is formed. Similarly, if the O_2 chemical potential is kept low and the H_2 chemical potential gradually increases (along the x-axis), the H-covered Pd(100) surface is

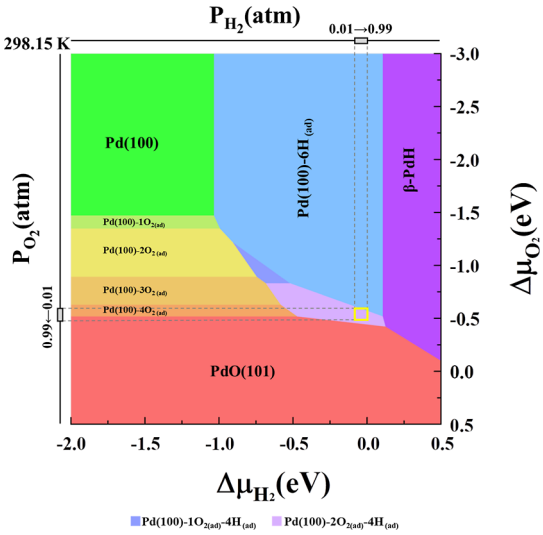

Figure 4. Surface phase diagram of Pd(100) in constrained thermodynamic equilibrium with gas-phase H_2 and O_2. The phase diagram is given considering the chemical potentials of H_2 and O_2. The corresponding H_2 and O_2 pressures at 298.15 K are shown in gray bars at the top and left of the axis. The yellow square in the phase diagram denotes the ambient conditions (0.01 bar < P_{O_2} < 0.99 bar, 0.01 bar < P_{H_2} < 0.99 bar).

first formed; thereafter, the β-phase palladium hydride ($PdH_{0.75}$) is formed. These results are in good agreement with the experimental results.[59]

The yellow square represents the region under ambient operating temperature and pressure. The region of the yellow square is situated in the phase of Pd(100)-$2O_{2(ad)}$-$4H_{(ad)}$ close to the boundary to Pd oxide and Pd hydride. Notably, the surface of Pd(100) is mainly occupied by O_2 (27.8%), H (43.3%), and free sites (28.7%) under ambient operating conditions (T = 298.15 K, P_{O_2} = P_{H_2} = 0.5 bar), which is consistent with the phase diagram of Pd(100).

3.2.4. Comparison of Intermediate Stabilities on the Three Surfaces. The stabilities of the intermediates[62,65,105] on Pd(100), Pd(111), and Pd(211) were described in detail to explore the influences of the lateral interaction on the three surfaces. The formula of intermediate stability is calculated as follows

$$E_{\text{stability}} = E_{\text{metal+adsorbate}} - a(E_{\text{metal+H}}) - b(E_{\text{metal+O}}) + (a + b - 1)\times E_{\text{metal}} \quad (9)$$

where $E_{\text{stability}}$ represents the relative stability of the intermediate on the surface, $E_{\text{metal+adsorbate}}$ is the free energy of the intermediate on the surface, $E_{\text{metal+H}}$ is the free energy of the most stable atomic H on the surface, $E_{\text{metal+O}}$ is the free energy of the most stable atomic O on the surface, a and b represent the numbers of H and O in the intermediates, and E_{metal} is the total energy of the surface of the corresponding transition metal.

As displayed in Figure 5, H, O, and OH are much more stable than O_2 and OOH with and without the coverage effect on Pd(100), Pd(111), and Pd(211). Hence, these three intermediates are very likely to occupy relatively large proportions of the surfaces, which is consistent with the coverage distribution. Furthermore, it is interesting to note that OH, O_2, and OOH with the coverage effect are more stable than those without the coverage effect on Pd(211), and the order of stability is OH > O

https://doi.org/10.1021/acscatal.3c03893
ACS Catal. 2023, 13, 15054−15073

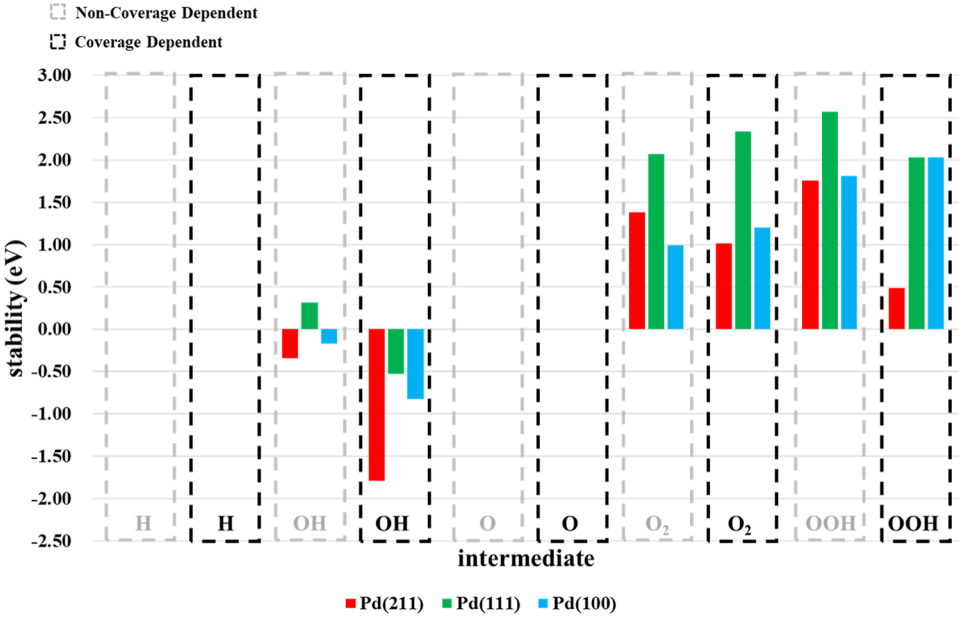

Figure 5. Stability bars of intermediates on Pd(100), Pd(111), and Pd(211) at 298.15 K. The large value of stability denotes less stability, and the small value of stability denotes excellent stability. The bars in black dashed line rectangular boxes represent stability with coverage effects, and the bars in gray dashed line boxes represent stability without coverage effects. The reaction conditions are $P_{O_2} = P_{H_2} = 0.5$ bar and $P_{H_2O_2} = P_{H_2O} = 0.035$ bar.

≈ H > OOH > O_2. Besides, OH and OOH exhibit higher stability when the lateral interactions are included, whereas O_2 becomes unstable on Pd(111), and the order of stabilities changes to OH > O ≈ H > OOH > O_2. On Pd(100), OH is much more stable with the coverage effect, but O_2 and OOH are much more unstable than those without the coverage effects. It is interesting to note that O_2 is more stable than OOH on Pd(100), which is different from the case for Pd(111) and Pd(211).

3.3. Detailed Analyses of the Mechanism of H_2O_2 and H_2O Formation on Pd(100), Pd(111), and Pd(211).

Detailed analyses of the three surfaces under various reaction conditions were performed. The activity is obtained by coverage-dependent kinetic modeling. $r_{H_2O_2}/(r_{H_2O_2} + r_{H_2O})$ was used to characterize the selectivity upon hydrogen peroxide production as follows

$$\text{selectivity}(i) = \frac{r_i}{\sum_i r_i} \tag{10}$$

where r_i is the reaction rate of species i, and $\sum_i r_i$ is the sum of the reaction rates of H_2O and H_2O_2.

3.3.1. Unravelling the H_2O_2 and H_2O Formation Mechanism and Detailed Analyses on Pd(100). 3.3.1.1. Effect of Temperature and Pressure on the Activity of Pd(100). Previous studies indicated that H_2O_2 synthesis and decomposition are affected by temperature and pressure.[36,59] In this work, we utilized the coverage-dependent kinetic model to investigate the activity of Pd(100) for H_2O_2 synthesis, H_2O formation, and H_2O_2 decomposition under various pressure and temperature conditions (Figure 6a−c). There is a cross point between the blue line (representing the activity of H_2O) and the red line (representing the activity of H_2O_2) when the pressure of O_2 is around 0.02 bar at a moderate temperature (T = 298.15 K, Figure 6d). The formation rate of H_2O is higher than that of H_2O_2 in the range of 0 bar < P_{O_2} < 0.02 bar. As the O_2 partial pressure continues to rise (0.02 bar < P_{O_2} < 0.7 bar), the formation rate of H_2O_2 reaches a maximum, followed by a slow decline (P_{O_2} > 0.7 bar).

It is known that higher concentrations of surface oxygen are related to enhanced H_2O_2 decomposition rates, but a mechanistic understanding of this relationship has not yet been established.[106,107] Our simulations indicate that the process of $H_2O_2 + * + * \rightarrow OH* + OH*$ is the major pathway for H_2O_2 decomposition. Additionally, the rates of H_2O_2 decomposition and H_2O formation are boosted by an increase in the oxygen partial pressure. It is worth noting that when the partial pressure of O_2 is greater than 0.9 bar, the purple line (H_2O_2 decomposition) and the blue line (H_2O formation) almost overlap, indicating that the formation rate of H_2O is approximately equal to the decomposition rate of H_2O_2. This result reveals that H_2O is mainly controlled by the decomposition of H_2O_2 (Figure S107). The corresponding reaction pathway is shown as follows: $H_2O_2 + * + * \rightarrow OH* + OH*$, $OH* + H* \rightarrow H_2O + * + *$ (P_{O_2} > 0.9 bar) [pathway (ii)]. When the O_2 partial pressure is lower than 0.9 bar, the reaction pathway is mainly controlled by $O_2* + * \rightarrow O* + O*$, $O* + H* \rightarrow OH*$, $OH* + H* \rightarrow H_2O + * + *$ [pathway (i)]. Furthermore, there is a turning point in the activity trend of H_2O at 323.15 K. The reason is that the reaction rate of pathway (i) increases first and then declines. In the range of 0.9−0.93 bar, the reaction rate of pathway (i) has begun to decline, while the rate of H_2O formation through pathway (ii) is far less than the decline rate, and pathway (ii) is still the major pathway of H_2O formation, making the formation rate of H_2O maintain a downward trend. When the oxygen partial pressure is larger than 0.93 bar, the formation rate of H_2O in pathway (ii) increases rapidly, which is much larger than that in pathway (i) and plays a dominant role, making the formation rate of H_2O continue to maintain an upward trend.

3.3.1.2. Effect of Temperature and Pressure on the Selectivity of Pd(100). Improving the selectivity of hydrogen peroxide production while ensuring high activity has long been a significant challenge in direct synthesis reactions. According to

https://doi.org/10.1021/acscatal.3c03893
ACS Catal. 2023, 13, 15054−15073

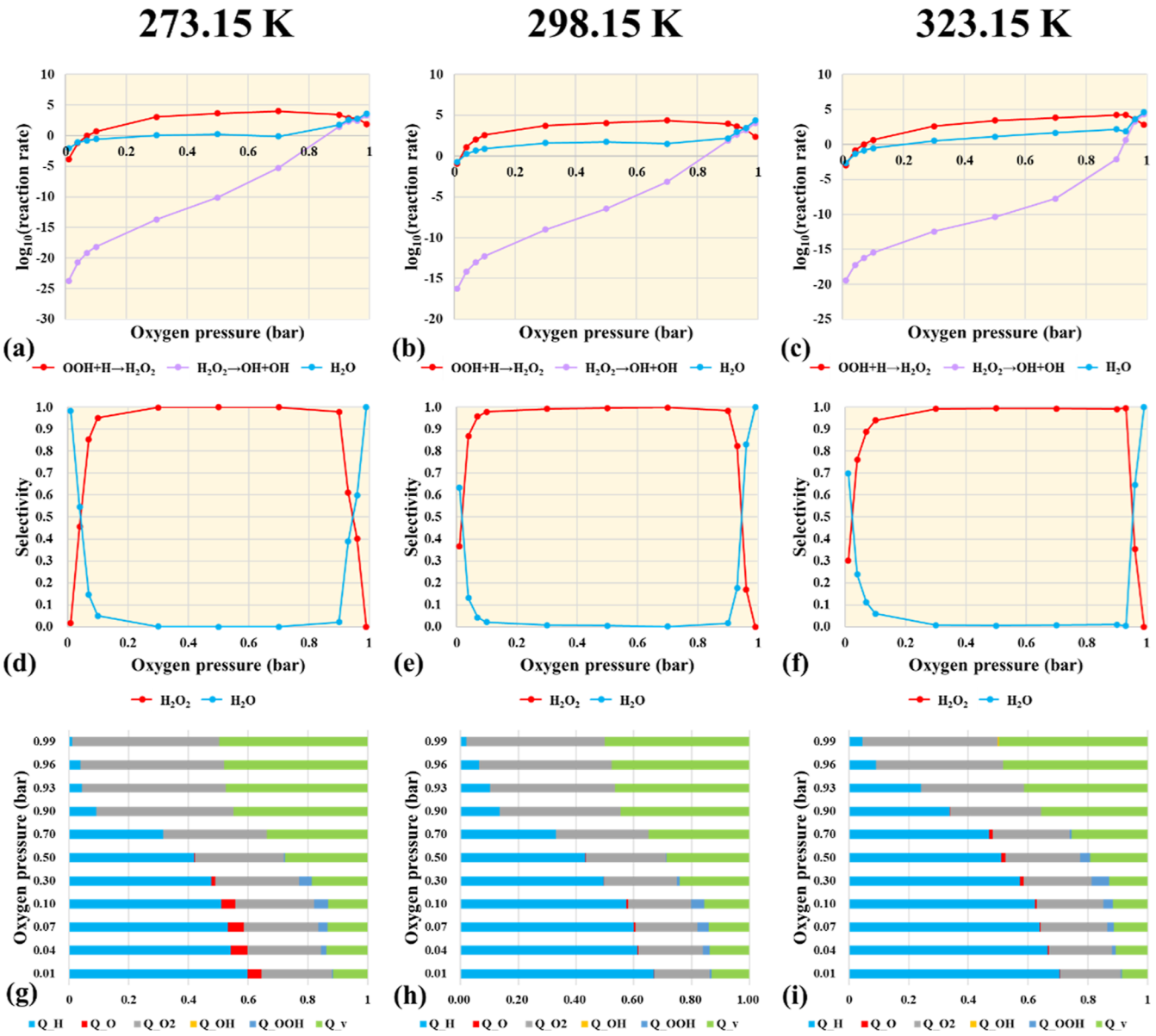

Figure 6. (a–c) Activity (OOH hydrogenation, H_2O_2 decomposition, and H_2O formation), (d-f) selectivity (H_2O_2 and H_2O), and (g–i) proportion of main species coverage on Pd(100) as a function of oxygen partial pressure from 273.15 to 323.15 K ($P_{O_2}+P_{H_2}$ = 1 bar, $P_{H_2O_2} = P_{H_2O}$ = 0.035 bar).

experimental reports,[108] the selectivity of H_2O_2 varied with the reactant ratio (H_2/O_2). To clarify the influence of temperature and pressure on selectivity, we chose three typical temperatures (273.15, 298.15, and 323.15 K) in our simulation. Figure 6 illustrates the influence of reaction conditions on H_2O_2 selectivity, from which the following features are striking. First, the selectivity of H_2O_2 initially increases and then decreases, while the selectivity of H_2O shows the opposite trend. Second, appropriate oxygen partial pressures, namely 0.3 bar < P_{O_2} < 0.7 bar (low temperature), 0.2 bar < P_{O_2} < 0.8 bar (moderate temperature), and 0.3 bar < P_{O_2} < 0.93 bar (high temperature) are beneficial to maintain the higher selectivity of hydrogen peroxide. At low pressure (0 bar < P_{O_2} < 0.1 bar), the H_2O_2 selectivity rises sharply with the increase in oxygen partial pressure. In the range of 0.9 bar < P_{O_2} < 0.99 bar, the selectivity of H_2O_2 descends rapidly. This is consistent with the experimental observation[28,58,109−111] that an excessively high or low reactant ratio (H_2/O_2) is not conducive to the formation of H_2O_2.

3.3.1.3. Effects of Temperature and Pressure on the Coverage of Pd(100). To understand the effects of pressure and temperature on the coverages of intermediates, we performed detailed coverage-dependent kinetic modeling analysis, and the surface species ratios are displayed in Figure 6g–i. Under the oxygen-lean condition, the Pd(100) surface is mainly covered by H, followed by O_2, while free sites constitute only a negligible fraction. With the enhancement of oxygen partial pressure, the proportion of H is decreased, and the proportion of O_2 and free sites is raised gradually. Under oxygen-rich conditions, the surface is mainly occupied by O_2 and free sites, and H is almost absent. In addition, the coverages of O and OOH occupy a very small portion of the surface at the oxygen-lean conditions (0.01 bar < P_{O_2} < 0.1 bar). As the O_2 pressure is increased (0.1 bar < P_{O_2} < 0.99 bar), O and OOH disappear. Furthermore, enriching the coverages of surface species H and

https://doi.org/10.1021/acscatal.3c03893
ACS Catal. 2023, 13, 15054−15073

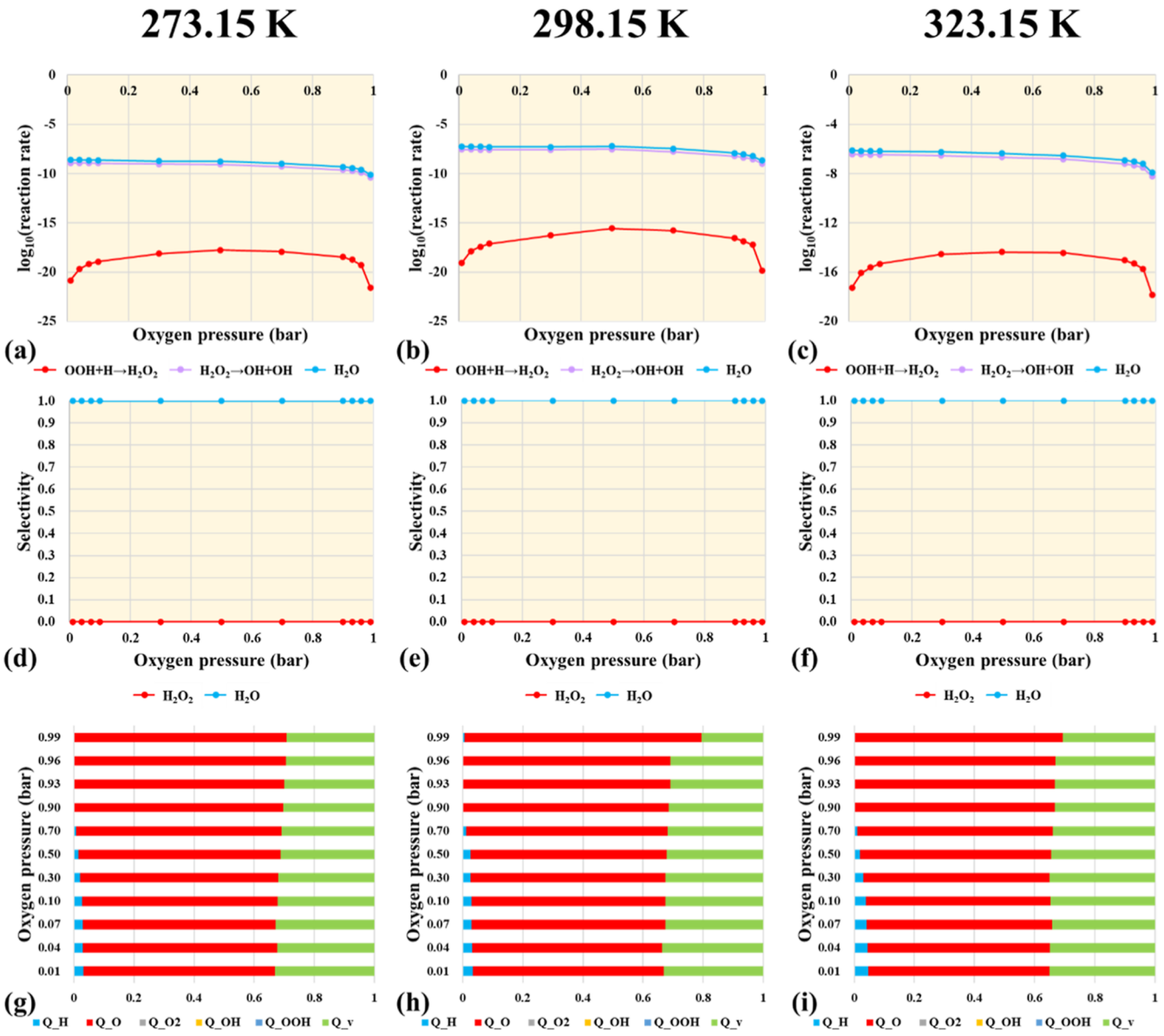

Figure 7. (a–c) Activity (OOH hydrogenation, H_2O_2 decomposition, and H_2O formation), (d–f) selectivity (H_2O_2 and H_2O), and (g–i) proportion of main species coverage on Pd(111) as a function of oxygen partial pressure from 273.15 to 323.15 K ($P_{O_2} + P_{H_2}$ = 1 bar, $P_{H_2O_2} = P_{H_2O}$ = 0.035 bar).

O_2 is beneficial to reduce the energy barrier of $O_2^* + H^* \rightarrow OOH^* + *$ and promote the formation of H_2O_2. It is worth mentioning that the free sites also play a significant role in the reaction process. In the absence of free sites, there will be fewer sites available for other intermediates to occupy, which inhibits the activity. Conversely, if there are excessive free sites, it will lead to the decomposition of H_2O_2, resulting in high selectivity of H_2O.

3.3.2. Unraveling the H_2O_2 and H_2O Formation Mechanism and Detailed Analyses on Pd(111). 3.3.2.1. Effect of Temperature and Pressure on the Activity on Pd(111). The Pd(111) surface mainly generates H_2O in the range of 0 bar < P_{O_2} < 0.99 bar (273.15–323.15 K). In the current work, we not only rigorously considered the effect of H_2O_2 dissociation ($H_2O_2 + * + * \rightarrow OH^* + OH^*$) but also took the influence of multiple species interactions into account and made the coverage self-consistent. As shown in Figure 7a–c, the rate of H_2O_2 rises in the range of 0.01 bar < P_{O_2} < 0.5 bar, and then it begins to decline. The rates of H_2O_2 decomposition and H_2O formation decrease with increasing O_2 pressure. It is worth noting that H_2O is generated by $H_2O_2 + * + * \rightarrow OH^* + OH^*$, $OH^* + H^* \rightarrow H_2O + * + *$, which means that the rate of H_2O_2 decomposition determines the activity of H_2O formation on Pd(111) and Pd(211).

3.3.2.2. Effect of Temperature and Pressure on the Selectivity of Pd(111). The selectivity of H_2O exhibits insensitivity to variations in temperature and pressure. This is due to the excessive free sites on the Pd(111) surface and the lack of crucial species H and O_2 (Figure 7d–f). A larger number of free sites will accelerate the process of $H_2O_2 + * + * \rightarrow OH^* + OH^*$, resulting in a significantly slower formation rate of H_2O_2 than the decomposition rate of H_2O_2 and contributing to the production of H_2O.

3.3.2.3. Effect of Temperature and Pressure on the Coverage on Pd(111). The surface of Pd(111) is mainly covered by free sites, while H occupies a very small fraction of the surface (Figure 7g–i). As the oxygen partial pressure rises

https://doi.org/10.1021/acscatal.3c03893
ACS Catal. 2023, 13, 15054–15073

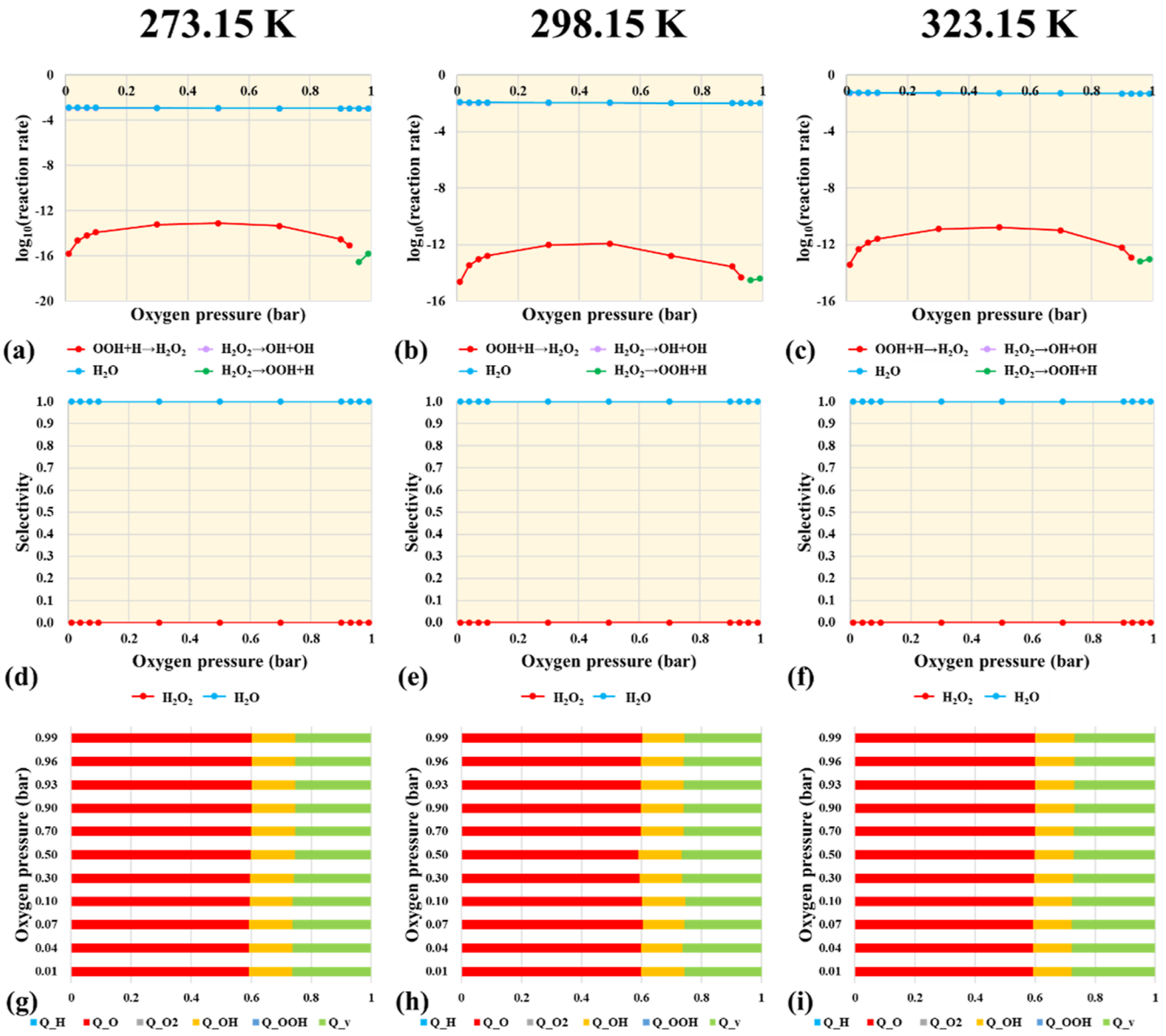

Figure 8. (a−c) Activity (OOH hydrogenation, H_2O_2 decomposition, and H_2O formation), (d−f) selectivity (H_2O_2 and H_2O), and (g−i) proportion of main species coverage on Pd(211) as a function of oxygen partial pressure from 273.15 to 323.15 K ($P_{O_2} + P_{H_2}$ = 1 bar, $P_{H_2O_2} = P_{H_2O}$ = 0.035 bar).

from 0.01 to 0.99 bar, the proportion of H and free sites gradually declines, while the proportion of O slightly increases. If the pressure is greater than 0.7 bar, there is little coverage occupied by H on the surface. Significantly, the activity of H_2O_2 decomposition is closely related to the proportion of free sites. With the increase in the oxygen partial pressure, the free sites are reduced, leading to a decrease in the rate of H_2O_2 decomposition.

3.3.3. Unravelling the H_2O_2 and H_2O Formation Mechanism and Detailed Analyses on Pd(211). 3.3.3.1. Effect of Temperature and Pressure on the Activity on Pd(211). The surface of Pd(211) is the major surface for H_2O_2 decomposition, as shown in Figure 8a−c. Both the activity of H_2O_2 decomposition and H_2O formation are found to be insensitive to the oxygen partial pressure. It is worth mentioning that the purple line (the H_2O_2 decomposition rate) almost completely overlaps with the blue line (the H_2O formation rate), indicating that the rate of H_2O generation is almost equal to the rate of H_2O_2 decomposition. The decomposition rate of H_2O_2 contributes to the dominant production of H_2O as the major product. Notably, when the oxygen partial pressure is greater than 0.93 bar, OOH hydrogenation is inhibited and $H_2O_2 + * + * \rightarrow OOH* + H*$ is accelerated.

3.3.3.2. Effect of Temperature and Pressure on Selectivity on Pd(211). On Pd(211), the selectivity of H_2O is found to be around 100% and temperature and pressure have little influence on the selectivity (Figure 8d−f). This result is similar to that on the Pd(111) surface. The reason is that the excessive free sites and the lack of key species H and O_2 make the formation rate of H_2O_2 much smaller than the decomposition rate of H_2O_2. Meanwhile, abundant OH can accelerate the process of $OH* + OH* \rightarrow H_2O + O* + *$.

3.3.3.3. Effect of Temperature and Pressure on the Coverage on Pd(211). It was found that the surface of Pd(211) is mainly covered by O (around 60%), followed by free sites (around 26%) and OH (around 14%), as shown in Figure 8g−i. The coverages of intermediates have an important influence on the activity and selectivity of H_2O_2. It was observed

https://doi.org/10.1021/acscatal.3c03893
ACS Catal. 2023, 13, 15054−15073

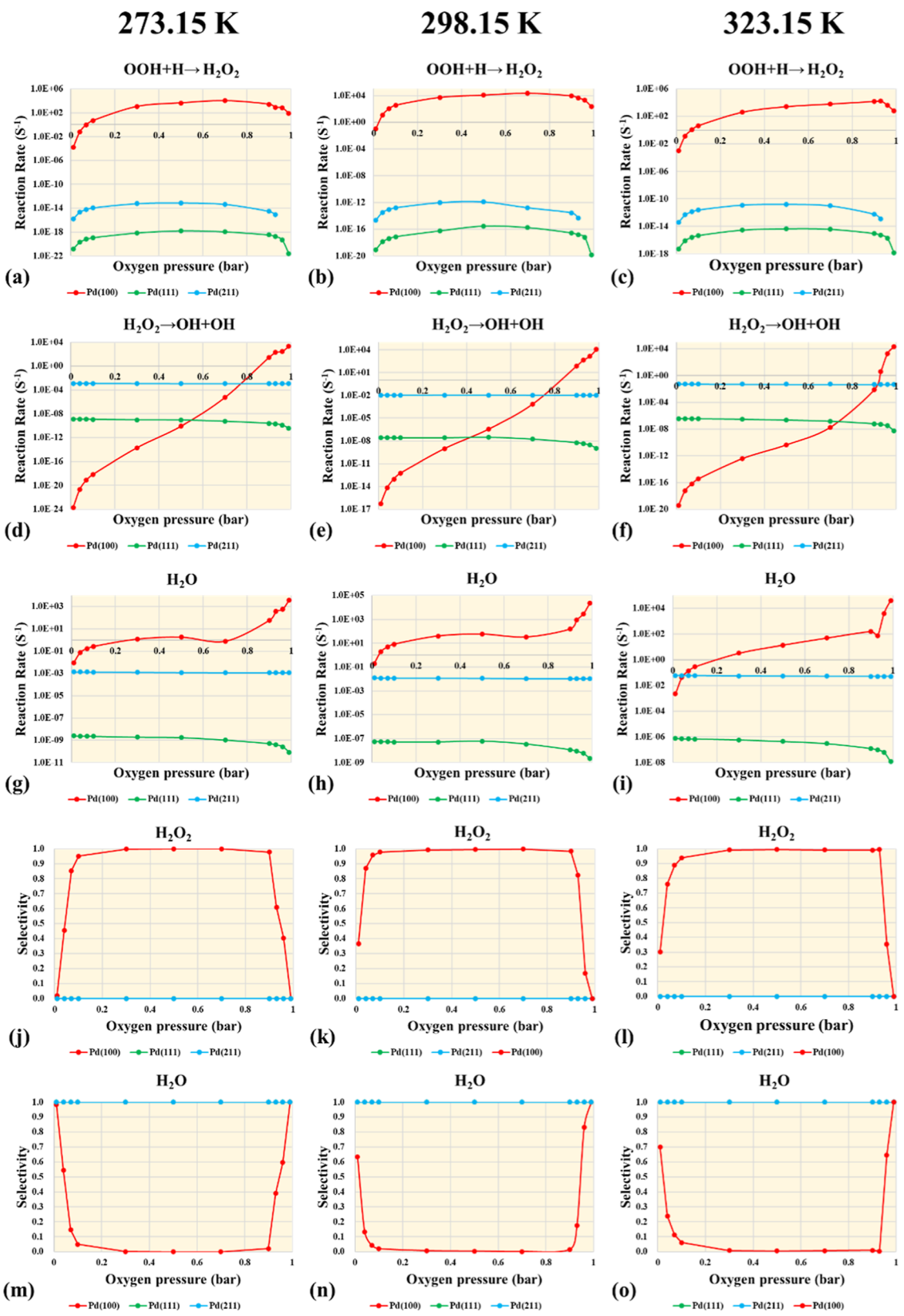

Figure 9. Comparison of (a−i) activity (OOH hydrogenation, H_2O_2 decomposition, and H_2O formation) and (j−o) selectivity (H_2O_2 and H_2O) as a function of oxygen partial pressure on Pd(100), Pd(111), and Pd(211) from 273.15 to 323.15 K. Red line is Pd(100), green line is Pd(111), and blue line is Pd(211) ($P_{O_2} + P_{H_2}$ = 1 bar, $P_{H_2O_2}$ = 0.035 bar).

that the variation of coverages is not sensitive to O_2 pressure, and the oxygen partial pressure has little influence on the selectivity of H_2O_2.

3.3.4. Activity and Selectivity Comparison on the Three Surfaces. In this section, we further compared the critical elementary reaction steps on the three surfaces to elucidate the

https://doi.org/10.1021/acscatal.3c03893
ACS Catal. 2023, 13, 15054−15073

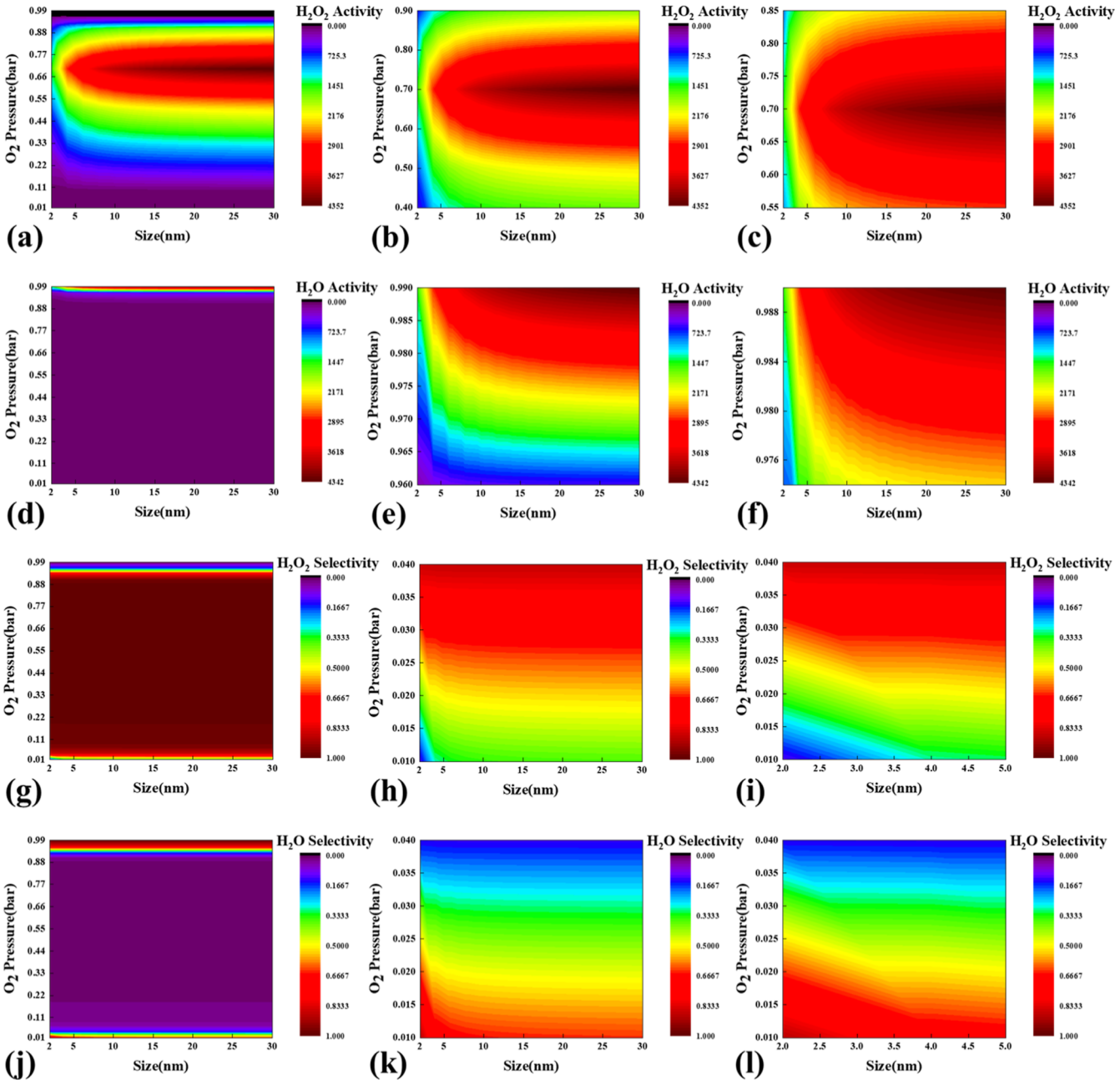

Figure 10. 2-D activity of (a−c) H_2O_2 and (d−f) H_2O heat map describing the values (reaction rate s^{-1}) on Pd nanoparticles as a function of oxygen partial pressure (0 bar < P_{O_2} < 1 bar) and size (2−30 nm); 2-D selectivity (g−i) H_2O_2 and (j−l) H_2O heat map on Pd nanoparticles as a function of (g) oxygen partial pressure (0 bar < P_{O_2} < 1 bar) and size (2−30 nm) (T = 298.15 K).

dominant sites and mechanisms for the direct synthesis of H_2O_2 (Figure 9).

First, the significant elementary step of H_2O_2 generation (OOH* + H* → H_2O_2 + * + *) was explored (Figure 9a−c). The reaction rate of OOH hydrogenation is in the order of Pd(100) > Pd(211) > Pd(111). It is worth noting that the OOH hydrogenation on Pd(211) does not occur when the oxygen partial pressure is greater than 0.93 bar. This result can be attributed to the fact that too little hydrogen causes the reaction to go backward.

Second, the key elementary reaction step of H_2O_2 decomposition (H_2O_2 + * + * → OH* + OH*) was investigated (Figure 9d−f). The decomposition rate of H_2O_2 on Pd(100) is lower than that on Pd(111) and Pd(211) in the range of 0 bar < P_{O_2} < 0.54 bar (low temperature), 0 bar < P_{O_2} < 0.42 bar (moderate temperature), 0 bar < P_{O_2} < 0.73 bar (high temperature). As the oxygen partial pressure continues to rise (0.54 bar < P_{O_2} < 0.76 bar at low temperature, 0.42 bar < P_{O_2} < 0.75 bar at moderate temperature, 0.73 bar < P_{O_2} < 0.92 bar at high temperature), the activity of Pd(100) for H_2O_2 decomposition gradually exceeds that on Pd(111) but is still less than that on Pd(211). When the oxygen partial pressure is larger than 0.76 bar (low temperature), 0.75 bar (moderate temperature), and 0.92 bar (high temperature), the H_2O_2 decomposition rate is in the order of Pd(100) > Pd(211) > Pd(111). It is worth mentioning that the H_2O_2 decomposition rate on Pd(211) is higher than that on Pd(111). Interestingly,

https://doi.org/10.1021/acscatal.3c03893
ACS Catal. 2023, 13, 15054−15073

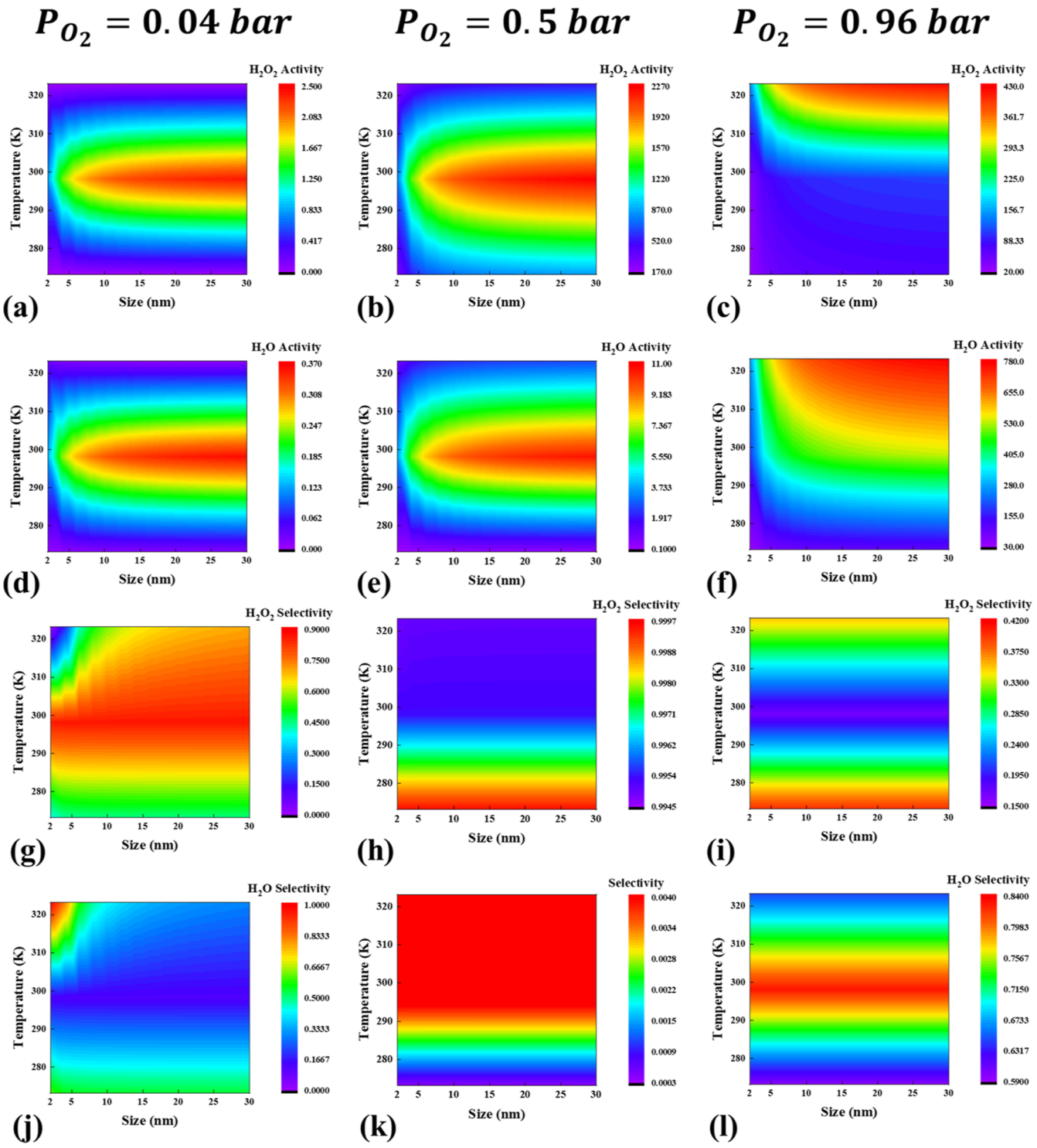

Figure 11. 2-D activity of (a–c) H_2O_2 and (d–f) H_2O heat map describing the values (reaction rate s^{-1}) on Pd nanoparticle as a function of size and temperature; 2-D selectivity of (g–i) H_2O_2 and (j–l) H_2O heat map on Pd nanoparticle as a function of size and temperature (P_{O_2} = 0.04 bar, P_{O_2} = 0.5 bar, and P_{O_2} = 0.96 bar).

the reaction rate of H_2O formation on Pd(100) is higher than those on Pd(111) and Pd(211) from low temperature to moderate temperature. However, there is a threshold point between Pd(100) and Pd(211) when the oxygen partial pressure is around 0.04 bar at high temperature. The H_2O formation rate on Pd(100) is lower than that on Pd(211) in the range of 0 bar < P_{O_2} < 0.04 bar, while the opposite result is observed in the range of 0.04 bar < P_{O_2} < 0.99 bar.

Finally, the selectivity of H_2O_2 and H_2O was analyzed under the influence of temperature and pressure (Figure 9j–o). The selectivity of H_2O on Pd(111) and Pd(211) is around 100%. The H_2O_2 selectivity on Pd(100) is always greater than that on Pd(111) and Pd(211) in the range of 0 bar < P_{O_2} < 1 bar, and this

https://doi.org/10.1021/acscatal.3c03893
ACS Catal. 2023, 13, 15054–15073

means that Pd(100) contains the dominant active site for generating H_2O_2.

3.4. Quantitative Determination of the H_2O_2 and H_2O Formation Mechanism Based on Microkinetic Modeling with Size-Dependent and Coverage Effects. Pd nanoparticles have been identified as the most effective catalyst for the direct synthesis of hydrogen peroxide, and their activity and selectivity strongly depend on the sizes of the Pd nanoparticles.[112] To simulate the size effect of Pd nanoparticles, microkinetic modeling with size-dependent and coverage effects was carried out.

3.4.1. Pressure Effect Using Microkinetic Modeling with Size-Dependent and Coverage Effects. Experiments demonstrated that the activity and selectivity of H_2O_2 can be improved by appropriately reducing the ratio of H_2/O_2.[113,114] On the other hand, H_2 selectivity toward H_2O_2 decreases with reducing the size of Pd particles.[28,109] Inspired by previous works,[28,59] we carried out the kinetic analysis, and the results are displayed in the 2-D selectivity heat map characterizing the values of selectivity and activity as a function of oxygen pressure and Pd nanoparticle size (Figure 10).

3.4.1.1. Activity Comparison with the Size Effect under Various Pressures. The influence of pressure on H_2O_2 and H_2O formation activity is evident from Figure 10a-f. The highest activity for H_2O_2 formation is observed at around 0.7 bar of O_2 pressure, with H_2O_2 formation rates sharply increasing in the range of 0 bar < P_{O_2} < 0.7 bar and beginning to decline from 0.7 to 1 bar. Interestingly, the trend of H_2O_2 activity on Pd nanoparticles is similar to the trend on Pd(100) (Figure S109). This similarity can be attributed to the activity of H_2O_2 on Pd(100) (10^4 s^{-1}) being higher than those observed on Pd(111) (10^{-15} s^{-1}) and Pd(211)(10^{-11} s^{-1}), despite its relatively low proportion on Pd nanoparticles (2−30 nm) (<20%). Furthermore, as the size of the Pd nanoparticle increases from 2 to 10 nm, the activity of H_2O_2 shows a sharp increase in the range of 0.4 bar < P_{O_2} < 0.9 bar. This enhancement is due to the proportion of Pd(100) rising from 6 to 17%. However, when the size of Pd nanoparticles further increases from 10 to 30 nm, the proportion of Pd(100) only increases by 2%, resulting in an insignificant change in activity.

3.4.1.2. Selectivity Comparison with the Size Effect under Various Pressures. The following features of reaction conditions on H_2O_2 and H_2O selectivity can be seen in Figure 10g−l. First, the selectivity of hydrogen peroxide is greater than that of water, constantly in the range of 0.02 bar < P_{O_2} < 0.945 bar. Second, when the oxygen partial pressure is in the range of 0 bar < P_{O_2} < 0.04 bar, the selectivity of hydrogen peroxide increases with the rise in size (from 2 to 5 nm). However, when the size is larger than 5 nm or the pressure of O_2 is greater than 0.04 bar, the Pd nanoparticle size has little influence on the selectivity of H_2O_2. Similarly, the selectivity of H_2O is sensitive to the size in the range of 0 bar < P_{O_2} < 0.04 bar (from 2 to 5 nm).

3.4.2. Temperature Effect Using Microkinetic Modeling with Size-Dependent and Coverage Effects. Temperature is another critical factor that affects the reaction rate. However, the mechanism of direct H_2O_2 synthesis remains elusive due to the limitations in both experimental and theoretical approaches.[36,113,115−117] In this work, we used the 2-D heat map to describe the values of selectivity and activity as a function of temperature and size (Figure 11).

3.4.2.1. Activity Comparison with the Size Effect from Low Temperature to High Temperature. The relationship between the size (2−30 nm) and the activity of H_2O_2 at various temperatures is investigated, and the results are shown in Figure 11a−f. When the oxygen partial pressure is around 0.04 bar, the formation rates of H_2O_2 and H_2O rise sharply in the temperature range of 273.15 K < T < 298.15 K, and then the activities of H_2O_2 and H_2O begin to decline from moderate temperature to high temperature. Similarly, the reaction rates of H_2O_2 and H_2O reach the optimum at moderate temperature under 0.5 bar oxygen pressure. This performance is consistent with the experimental results of Pashkova and co-workers,[115] who found that the yield of H_2O_2 was higher at 27 °C than at 40°. It is worth mentioning that the formation rate of H_2O_2 is larger than that of H_2O at 0.04 and 0.5 bar. However, the reaction rates of H_2O_2 and H_2O formation are boosted with an increase in temperature at an oxygen partial pressure of 0.96 bar.

Additionally, as the size of the Pd nanoparticle increases, the activity of H_2O_2 and H_2O significantly improves from 2 to 10 nm. While the size is larger than 10 nm, the rates of H_2O_2 and H_2O formation grow slowly.

3.4.2.2. Selectivity Comparison with the Size Effect from Low Temperature to High Temperature. To clarify the influence of size on the selectivity of H_2O_2 and H_2O at different temperatures, we carried out the kinetic analysis, and the results are displayed in the 2-D selectivity heat map, characterizing the selectivity as a function of size and temperature (Figure 11g−l).

It can be observed that the selectivity of H_2O_2 increases from low temperature to moderate temperature (oxygen-lean conditions, P_{O_2} = 0.04 bar). Experimentally, Shi et al.[36] found a strong increase in H_2O_2 selectivity with a temperature rise at low temperature. This result can be attributed to the fact that the formation rate of H_2O_2 is growing faster than that of H_2O from low temperature to moderate temperature. Under balanced conditions (P_{O_2} = 0.5 bar), low temperature is beneficial to maintain a higher selectivity of hydrogen peroxide. Biasi et al.[116] studied the effect of temperature (−5, 0, 10, and 40 °C) on the direct synthesis of H_2O_2 by using a batch reactor and methanol solvent. The selectivity of H_2O_2 was observed to decrease with rising temperatures, which is consistent with our simulation. Under oxygen-rich conditions (P_{O_2} = 0.96 bar), the selectivity of H_2O_2 decreases from low to moderate temperature, while the opposite trend is observed from moderate to high temperature. The reason is that the rate increase of H_2O_2 formation is faster than that of H_2O formation in the range of 273.15 K < T < 298.15 K, once the temperature is higher than 298.15 K; the enhancement in H_2O_2 formation rate is more significant (Figure S108).

In addition, as the size of Pd nanoparticles rises, the selectivity of H_2O_2 increases sharply from 2 to 10 nm in the range of 298.15 K < T < 323.15 K under oxygen-lean conditions (P_{O_2} = 0.04 bar). Smaller sizes with more edge are beneficial to H_2O_2 decomposition, and large sizes with more terrace sites are favorable for H_2O_2 formation. On the other hand, the selectivity of H_2O_2 and H_2O is not sensitive to the size in the pressure range of 0.5 to 0.96 bar. This means that when the oxygen partial pressure is larger than 0.5 bar, the temperature is the major factor for the selectivity of H_2O_2 rather than the Pd nanoparticle size.

https://doi.org/10.1021/acscatal.3c03893
ACS Catal. 2023, 13, 15054−15073

4. CONCLUSIONS

This work develops an advanced microkinetic modeling with the adsorbate−adsorbate interaction and nanoparticle size effect based on first-principles calculations that considers all of the vital issues that can affect the rate of a metal nanoparticle catalyst. The following major conclusions are obtained:

(i) Among the three surfaces, Pd(100) has the optimum hydrogen peroxide formation activity (10^4 s^{-1}) at moderate temperature. This activity level is much higher than that observed on Pd(111) (10^{-15} s^{-1}) and Pd(211) (10^{-11} s^{-1}), making Pd(100) the major active site for H_2O_2 generation. Pd(111) and Pd(211) contain the active sites of hydrogen peroxide decomposition, and the decomposition rate of Pd(211) (10^{-2} s^{-1}) is higher than that of Pd(111) (10^{-7} s^{-1}).

(ii) The adsorbate−adsorbate interactions considerably affect the reaction mechanism for the direct synthesis of hydrogen peroxide on the three surfaces. The species of O_2 and H on Pd(100) can promote O_2 and OOH hydrogenation and inhibit H_2O_2 decomposition. However, Pd(111) covered by O and Pd(211) covered by O and OH are beneficial to H_2O formation.

(iii) The variation in reaction temperature will make the proportions of intermediates change, but it has little effect on the major types of surface species. In the temperature range of 273.15 K < T < 323.15 K, the coverage of O_2 slowly reduces and H gradually increases on Pd(100) with the increase of temperature. While the coverage of free sites initially rises in the range of 273.15 K < T < 298.15 K, followed by a dramatical decline (298.15 K < T < 323.15 K). The trend of activity is consistent with that of free sites, and H_2O_2 is the major product.

(iv) The ratio of H_2/O_2 partial pressure possesses great effects on surface coverages on Pd(100). The H_2O_2 selectivity is more sensitive to the change in the ratio of partial pressures than the temperature. Under oxygen-lean conditions, the coverage of H is high, and the proportions of O_2 and free sites are lower, resulting in poor activity and selectivity of H_2O_2. While under oxygen-rich conditions, the proportions of O_2 and free sites are high, and the proportion of H is lower. The higher proportion of free sites is conducive to the decomposition of H_2O_2. The decomposition rate of H_2O_2 is larger than the formation rate of H_2O_2, contributing to improving the yield of H_2O.

(v) The two-dimensional selectivity and activity heat maps as a function of Pd particle size and temperature/pressure deepen our understanding of the mechanism with the coverage effects. Based on the current data, the microkinetic modeling with size-dependent and coverage effects can help us predict the optimal reaction conditions (temperature and pressure) with various sizes. When the temperature is around 298.15 K and the oxygen partial pressure is around 0.7 bar, the activity and selectivity of hydrogen peroxide synthesis reach the highest level on the large size of Pd nanoparticles.

■ ASSOCIATED CONTENT

Supporting Information

The Supporting Information is available free of charge at https://pubs.acs.org/doi/10.1021/acscatal.3c03893.

Computational methods; generalized formation energy formulas; flow diagram of microkinetic modeling; relationship with size and different proportion of Pd nanoparticles; barriers and reaction energies of elementary reactions on Pd(100) and Pd(111) without the coverage effect; intermediates and transition states under H, O, and O_2 environments on Pd(100) and Pd(211); energy profiles for the formation of H_2O_2 and H_2O and decomposition of H_2O_2 on Pd(100), Pd(211), and Pd(111); barriers and reaction energies of elementary reactions on Pd(211) and Pd(111) with the coverage effect; . 2D H_2O_2 activity heat maps; optimized geometries of intermediates; and production rates of H_2O_2 and H_2O (PDF)

■ AUTHOR INFORMATION

Corresponding Authors

Zihao Yao − *Institute of Industrial Catalysis, College of Chemical Engineering, Zhejiang University of Technology, Hangzhou 310032, People's Republic of China;* orcid.org/0000-0001-5259-6609; Email: yaozihao@zjut.edu.cn

P. Hu − *Institute of Industrial Catalysis, College of Chemical Engineering, Zhejiang University of Technology, Hangzhou 310032, People's Republic of China; School of Physical Science and Technology, ShanghaiTech University, Shanghai 201210, China;* orcid.org/0000-0002-6318-1051; Email: p.hu@qub.ac.uk

Jianguo Wang − *Institute of Industrial Catalysis, College of Chemical Engineering, Zhejiang University of Technology, Hangzhou 310032, People's Republic of China;* orcid.org/0000-0003-2391-4529; Email: jgw@zjut.edu.cn

Authors

Jinyan Zhao − *Institute of Industrial Catalysis, College of Chemical Engineering, Zhejiang University of Technology, Hangzhou 310032, People's Republic of China*

Rhys J. Bunting − *School of Chemistry and Chemical Engineering, The Queen's University of Belfast, Belfast BT9 5AG, U.K.; Institute of Science and Technology Austria, 3400 Klosterneuburg, Austria;* orcid.org/0000-0001-6928-074X

Complete contact information is available at: https://pubs.acs.org/10.1021/acscatal.3c03893

Author Contributions

⊥J.Z. and Z.Y. contributed equally.

Notes

The authors declare no competing financial interest.

■ ACKNOWLEDGMENTS

The authors acknowledge the financial support from the National Natural Science Foundation of China (22008211, 92045303, U21A20298), the National Key Research and Development Project of China (2021YFA1500900, 2022YFE0113800), and Zhejiang Innovation Team (2017R5203).

■ REFERENCES

(1) Campos-Martin, J. M.; Blanco-Brieva, G.; Fierro, J. L. Hydrogen peroxide synthesis: an outlook beyond the anthraquinone process. *Angew. Chem., Int. Ed. Engl.* **2006**, *45* (42), 6962−6984.

(2) Perry, S. C.; Pangotra, D.; Vieira, L.; Csepei, L.-I.; Sieber, V.; Wang, L.; Ponce de León, C.; Walsh, F. C. Electrochemical synthesis of hydrogen peroxide from water and oxygen. *Nat. Rev. Chem* **2019**, *3* (7), 442−458.

(3) Agarwal, N.; Freakley, S. J.; McVicker, R. U.; Althahban, S. M.; Dimitratos, N.; He, Q.; Morgan, D. J.; Jenkins, R. L.; Willock, D. J.; Taylor, S. H.; Kiely, C. J.; Hutchings, G. J. Aqueous Au-Pd colloids catalyze selective CH_4 oxidation to CH_3OH with O_2 under mild conditions. *Science* **2017**, *358* (6360), 223−227.
(4) Xia, C.; Xia, Y.; Zhu, P.; Fan, L.; Wang, H. Direct electrosynthesis of pure aqueous H_2O_2 solutions up to 20% by weight using a solid electrolyte. *Science* **2019**, *366* (6462), 226−231.
(5) Hans-joachim, R.; Georg, P. Production of hydrogen peroxide. U.S. Patent . 2,158,525 A, 1939.
(6) Paunovic, V.; Ordomsky, V.; Fernanda Neira D'Angelo, M.; Schouten, J. C.; Nijhuis, T. A. Direct synthesis of hydrogen peroxide over Au-Pd catalyst in a wall-coated microchannel. *J. Catal.* **2014**, *309*, 325−332.
(7) Quon, S.; Jo, D. Y.; Han, G.-H.; Han, S. S.; Seo, M.-g.; Lee, K.-Y. Role of Pt atoms on Pd(111) surface in the direct synthesis of hydrogen peroxide: Nano-catalytic experiments and DFT calculations. *J. Catal.* **2018**, *368*, 237−247.
(8) Biasi, P.; Mikkola, J. P.; Sterchele, S.; Salmi, T.; Gemo, N.; Shchukarev, A.; Centomo, P.; Zecca, M.; Canu, P.; Rautio, A. R.; Kordàs, K. Revealing the role of bromide in the H_2O_2 direct synthesis with the catalyst wet pretreatment method (CWPM). *AIChE J.* **2017**, *63* (1), 32−42.
(9) Xu, H.; Cheng, D.; Gao, Y. Design of High-Performance Pd-Based Alloy Nanocatalysts for Direct Synthesis of H_2O_2. *ACS Catal.* **2017**, *7* (3), 2164−2170.
(10) Arrigo, R.; Schuster, M. E.; Abate, S.; Giorgianni, G.; Centi, G.; Perathoner, S.; Wrabetz, S.; Pfeifer, V.; Antonietti, M.; Schlögl, R. Pd Supported on Carbon Nitride Boosts the Direct Hydrogen Peroxide Synthesis. *ACS Catal.* **2016**, *6* (10), 6959−6966.
(11) Ciriminna, R.; Albanese, L.; Meneguzzo, F.; Pagliaro, M. Hydrogen Peroxide: A Key Chemical for Today's Sustainable Development. *ChemSusChem* **2016**, *9* (24), 3374−3381.
(12) Tian, P.; Ouyang, L.; Xu, X.; Ao, C.; Xu, X.; Si, R.; Shen, X.; Lin, M.; Xu, J.; Han, Y.-F. The origin of palladium particle size effects in the direct synthesis of H2O2: Is smaller better? *J. Catal.* **2017**, *349*, 30−40.
(13) Tian, P.; Ouyang, L.; Xu, X.; Xu, J.; Han, Y.-F. Density functional theory study of direct synthesis of H2O2 from H2 and O2 on Pd(111), Pd(100), and Pd(110) surfaces. *Chin. J. Catal.* **2013**, *34* (5), 1002−1012.
(14) Jeong, H. E.; Kim, S.; Seo, M.-g.; Lee, D.-W.; Lee, K.-Y. Catalytic activity of Pd octahedrons/SiO_2 for the direct synthesis of hydrogen peroxide from hydrogen and oxygen. *J. Mol. Catal. A: Chem.* **2016**, *420*, 88−95.
(15) Puértolas, B.; Hill, A. K.; García, T.; Solsona, B.; Torrente-Murciano, L. In-situ synthesis of hydrogen peroxide in tandem with selective oxidation reactions: A mini-review. *Catal. Today* **2015**, *248*, 115−127.
(16) Seo, M.-g.; Kim, H. J.; Han, S. S.; Lee, K.-Y. Direct Synthesis of Hydrogen Peroxide from Hydrogen and Oxygen Using Tailored Pd Nanocatalysts: A Review of Recent Findings. *Catal. Surv. Asia* **2017**, *21* (1), 1−12.
(17) Chen, W.; Ji, J.; Feng, X.; Duan, X.; Qian, G.; Li, P.; Zhou, X.; Chen, D.; Yuan, W. Mechanistic insight into size-dependent activity and durability in Pt/CNT catalyzed hydrolytic dehydrogenation of ammonia borane. *J. Am. Chem. Soc.* **2014**, *136* (48), 16736−16739.
(18) Rahm, J. M.; Erhart, P. Beyond Magic Numbers: Atomic Scale Equilibrium Nanoparticle Shapes for Any Size. *Nano Lett.* **2017**, *17* (9), 5775−5781.
(19) Kaden, W. E.; Wu, T.; Kunkel, W. A.; Anderson, S. L. Electronic structure controls reactivity of size-selected Pd clusters adsorbed on TiO_2 surfaces. *Science* **2009**, *326* (5954), 826−829.
(20) Campbell, C. T. The energetics of supported metal nanoparticles: relationships to sintering rates and catalytic activity. *Acc. Chem. Res.* **2013**, *46* (8), 1712−1719.
(21) Freakley, S. J.; He, Q.; Harrhy, J. H.; Lu, L.; Crole, D. A.; Morgan, D. J.; Ntainjua, E. N.; Edwards, J. K.; Carley, A. F.; Borisevich, A. Y.; Kiely, C. J.; Hutchings, G. J. Palladium-tin catalysts for the direct synthesis of H_2O_2 with high selectivity. *Science* **2016**, *351* (6276), 965−968.
(22) Menegazzo, F.; Signoretto, M.; Frison, G.; Pinna, F.; Strukul, G.; Manzoli, M.; Boccuzzi, F. When high metal dispersion has a detrimental effect: Hydrogen peroxide direct synthesis under very mild and nonexplosive conditions catalyzed by Pd supported on silica. *J. Catal.* **2012**, *290*, 143−150.
(23) Kim, S.; Lee, D.-W.; Lee, K.-Y.; Cho, E. A. Effect of Pd Particle Size on the Direct Synthesis of Hydrogen Peroxide from Hydrogen and Oxygen over Pd Core-Porous SiO_2 Shell Catalysts. *Catal. Lett.* **2014**, *144* (5), 905−911.
(24) Liu, P.; Lin, Q.; Pan, H.; Zhao, J.; Zhao, C.; Wang, Y. Direct synthesis of hydrogen peroxide from hydrogen and oxygen over yolk-shell nanocatalyst Pd@HCS with controlled Pd nanoparticle size. *J. Catal.* **2019**, *377*, 511−523.
(25) Deguchi, T.; Iwamoto, M. Catalytic Properties of Surface Sites on Pd Clusters for Direct H_2O_2 Synthesis from H_2 and O_2: A DFT Study. *J. Phys. Chem. C* **2013**, *117* (36), 18540−18548.
(26) Tian, P.; Ding, D.; Sun, Y.; Xuan, F.; Xu, X.; Xu, J.; Han, Y.-F. Theoretical study of size effects on the direct synthesis of hydrogen peroxide over palladium catalysts. *J. Catal.* **2019**, *369*, 95−104.
(27) Tian, P.; Xuan, F.; Ding, D.; Sun, Y.; Xu, X.; Li, W.; Si, R.; Xu, J.; Han, Y.-F. Revealing the role of tellurium in palladium-tellurium catalysts for the direct synthesis of hydrogen peroxide. *J. Catal.* **2020**, *385*, 21−29.
(28) Wilson, N. M.; Flaherty, D. W. Mechanism for the Direct Synthesis of H_2O_2 on Pd Clusters: Heterolytic Reaction Pathways at the Liquid-Solid Interface. *J. Am. Chem. Soc.* **2016**, *138* (2), 574−586.
(29) Chinta, S. A mechanistic study of H_2O_2 and H_2O formation from H_2 and O_2 catalyzed by palladium in an aqueous medium. *J. Catal.* **2004**, *225* (1), 249−255.
(30) Gervasini, A.; Carniti, P.; Desmedt, F.; Miquel, P. Liquid Phase Direct Synthesis of H_2O_2: Activity and Selectivity of Pd-Dispersed Phase on Acidic Niobia-Silica Supports. *ACS Catal.* **2017**, *7* (7), 4741−4752.
(31) Adams, J. S.; Chemburkar, A.; Priyadarshini, P.; Ricciardulli, T.; Lu, Y.; Maliekkal, V.; Sampath, A.; Winikoff, S.; Karim, A. M.; Neurock, M.; Flaherty, D. W. Solvent molecules form surface redox mediators in situ and cocatalyze O_2 reduction on Pd. *Science* **2021**, *371* (6529), 626−632.
(32) Yi, Y.; Wang, L.; Yu, J.; Guo, H.; Zhang, J.; Meng, C. The promotion of Argon and water molecule on direct synthesis of H_2O_2 from H_2 and O_2. *AIChE J.* **2018**, *64* (3), 981−992.
(33) Zhang, X.; Zhao, X.; Zhu, P.; Adler, Z.; Wu, Z. Y.; Liu, Y.; Wang, H. Electrochemical oxygen reduction to hydrogen peroxide at practical rates in strong acidic media. *Nat. Commun.* **2022**, *13* (1), 2880.
(34) Chen, L.; Moura, P.; Medlin, J. W.; Gronbeck, H. Multiple Roles of Alkanethiolate-Ligands in Direct Formation of H_2O_2 over Pd Nanoparticles. *Angew. Chem., Int. Ed. Engl.* **2022**, *134* (51), No. e202213113.
(35) Wang, S.; Jiang, G.; Yang, Z.; Mu, L.; Ji, T.; Lu, X.; Zhu, J. Boosted H_2O_2 Productivity by Sulfur-Doped Pd/Carbon Catalysts via Direct Synthesis from H_2 and O_2 at Atmospheric Pressure. *ACS Sustainable Chem. Eng.* **2022**, *10* (41), 13750−13758.
(36) Shi, L.; Goldbach, A.; Zeng, G.; Xu, H. Direct H_2O_2 synthesis over Pd membranes at elevated temperatures. *J. Membr. Sci.* **2010**, *348* (1−2), 160−166.
(37) Zhang, L.; Chen, D.; Jiang, Z.; Zhang, J.; Xie, S.; Kuang, Q.; Xie, Z.; Zheng, L. Facile syntheses and enhanced electrocatalytic activities of Pt nanocrystals with {hkk} high-index surfaces. *Nano Res.* **2012**, *5* (3), 181−189.
(38) Turner, M.; Golovko, V. B.; Vaughan, O. P.; Abdulkin, P.; Berenguer-Murcia, A.; Tikhov, M. S.; Johnson, B. F.; Lambert, R. M. Selective oxidation with dioxygen by gold nanoparticle catalysts derived from 55-atom clusters. *Nature* **2008**, *454* (7207), 981−983.
(39) Valden, M.; Lai, X.; Goodman, D. W. Onset of catalytic activity of gold clusters on titania with the appearance of nonmetallic properties. *Science* **1998**, *281* (5383), 1647−1650.

https://doi.org/10.1021/acscatal.3c03893
ACS Catal. 2023, 13, 15054−15073

(40) Chen, W.; Ji, J.; Duan, X.; Qian, G.; Li, P.; Zhou, X.; Chen, D.; Yuan, W. Unique reactivity in Pt/CNT catalyzed hydrolytic dehydrogenation of ammonia borane. *Chem. Commun.* **2014**, *50* (17), 2142−2144.
(41) Lyu, J.; Wang, J.; Lu, C.; Ma, L.; Zhang, Q.; He, X.; Li, X. Size-Dependent Halogenated Nitrobenzene Hydrogenation Selectivity of Pd Nanoparticles. *J. Phys. Chem. C* **2014**, *118* (5), 2594−2601.
(42) Crespo-Quesada, M.; Yarulin, A.; Jin, M.; Xia, Y.; Kiwi-Minsker, L. Structure sensitivity of alkynol hydrogenation on shape- and size-controlled palladium nanocrystals: which sites are most active and selective? *J. Am. Chem. Soc.* **2011**, *133* (32), 12787−12794.
(43) Genest, A.; Silvestre-Albero, J.; Li, W. Q.; Rosch, N.; Rupprechter, G. The origin of the particle-size-dependent selectivity in 1-butene isomerization and hydrogenation on Pd/Al_2O_3 catalysts. *Nat. Commun.* **2021**, *12* (1), 6098.
(44) Spencer, N. D.; Schoonmaker, R. C.; Somorjai, G. A. Structure sensitivity in the iron single-crystal catalysed synthesis of ammonia. *Nature* **1981**, *294* (5842), 643−644.
(45) Han, G. H.; Lee, S. H.; Hwang, S. Y.; Lee, K. Y. Advanced Development Strategy of Nano Catalyst and DFT Calculations for Direct Synthesis of Hydrogen Peroxide. *Adv. Energy Mater.* **2021**, *11* (27), 2003121.
(46) Lee, M. W.; Jo, D. Y.; Han, G.-H.; Lee, K.-Y. DFT calculations on selectivity enhancement by Br addition on Pd catalysts in the direct synthesis of hydrogen peroxide. *Catal. Today* **2022**, *397−399*, 232−239.
(47) Yang, X.-j.; Tian, P.-f.; Wang, H.-l.; Xu, J.; Han, Y.-f. Catalytic decomposition of H_2O_2 over a Au/carbon catalyst: A dual intermediate model for the generation of hydroxyl radicals. *J. Catal.* **2016**, *336*, 126−132.
(48) Rossi, U.; Zancanella, S.; Artiglia, L.; Granozzi, G.; Canu, P. Direct synthesis of H_2O_2 on model Pd surfaces. *Chem. Eng. J.* **2012**, *207−208*, 845−850.
(49) Shi, Y.; Elnabawy, A. O.; Gilroy, K. D.; Hood, Z. D.; Chen, R.; Wang, C.; Mavrikakis, M.; Xia, Y. Decomposition Kinetics of H_2O_2 on Pd Nanocrystals with Different Shapes and Surface Strains. *ChemCatChem* **2022**, *14* (16), No. e202200475.
(50) Cai, Q.-X.; Wang, J.-G.; Wang, Y.-G.; Mei, D. Mechanistic insights into the structure-dependent selectivity of catalytic furfural conversion on platinum catalysts. *AIChE J.* **2015**, *61* (11), 3812−3824.
(51) Yang, F.; Liu, D.; Zhao, Y.; Wang, H.; Han, J.; Ge, Q.; Zhu, X. Size Dependence of Vapor Phase Hydrodeoxygenation of m-Cresol on Ni/SiO_2 Catalysts. *ACS Catal.* **2018**, *8* (3), 1672−1682.
(52) Mahata, A.; Rawat, K. S.; Choudhuri, I.; Pathak, B. Cuboctahedral vs. octahedral platinum nanoclusters: insights into the shape-dependent catalytic activity for fuel cell applications. *Catal. Sci. Technol.* **2016**, *6* (21), 7913−7923.
(53) Mark, L. O.; Zhu, C.; Medlin, J. W.; Heinz, H. Understanding the Surface Reactivity of Ligand-Protected Metal Nanoparticles for Biomass Upgrading. *ACS Catal.* **2020**, *10* (10), 5462−5474.
(54) Li, J.; Yao, Z.; Zhao, J.; Deng, S.; Wang, S.; Wang, J. Microkinetic simulations of acetylene(acetylene-d2) hydrogenation(deuteration) on Ag nanoparticles. *Mol. Catal.* **2023**, *535*, 112845.
(55) Yang, N.; Medford, A. J.; Liu, X.; Studt, F.; Bligaard, T.; Bent, S. F.; Norskov, J. K. Intrinsic Selectivity and Structure Sensitivity of Rhodium Catalysts for C_{2+} Oxygenate Production. *J. Am. Chem. Soc.* **2016**, *138* (11), 3705−3714.
(56) Grabow, L. C.; Hvolbæk, B.; Nørskov, J. K. Understanding Trends in Catalytic Activity: The Effect of Adsorbate-Adsorbate Interactions for CO Oxidation Over Transition Metals. *Top. Catal.* **2010**, *53* (5−6), 298−310.
(57) He, Y.; Liu, J. C.; Luo, L.; Wang, Y. G.; Zhu, J.; Du, Y.; Li, J.; Mao, S. X.; Wang, C. Size-dependent dynamic structures of supported gold nanoparticles in CO oxidation reaction condition. *Proc. Natl. Acad. Sci. U.S.A.* **2018**, *115* (30), 7700−7705.
(58) Kanungo, S.; van Haandel, L.; Hensen, E. J. M.; Schouten, J. C.; Neira d'Angelo, M. F. Direct synthesis of H2O2 in AuPd coated micro channels: An in-situ X-Ray absorption spectroscopic study. *J. Catal.* **2019**, *370*, 200−209.
(59) Selinsek, M.; Deschner, B. J.; Doronkin, D. E.; Sheppard, T. L.; Grunwaldt, J.-D.; Dittmeyer, R. Revealing the Structure and Mechanism of Palladium during Direct Synthesis of Hydrogen Peroxide in Continuous Flow Using Operando Spectroscopy. *ACS Catal.* **2018**, *8* (3), 2546−2557.
(60) Song, X.; Sun, K.; Hao, X.; Su, H.-Y.; Ma, X.; Xu, Y. Facet-Dependent of Catalytic Selectivity: The Case of H_2O_2 Direct Synthesis on Pd Surfaces. *J. Phys. Chem. C* **2019**, *123* (43), 26324−26337.
(61) Plauck, A.; Stangland, E. E.; Dumesic, J. A.; Mavrikakis, M. Active sites and mechanisms for H_2O_2 decomposition over Pd catalysts. *Proc. Natl. Acad. Sci. U.S.A.* **2016**, *113* (14), No. E1973.
(62) Yao, Z. H.; Zhao, J. Y.; Bunting, R. J.; Zhao, C. X.; Hu, P. J.; Wang, J. G. Quantitative Insights into the Reaction Mechanism for the Direct Synthesis of H_2O_2 over Transition Metals: Coverage-Dependent Microkinetic Modeling. *ACS Catal.* **2021**, *11* (3), 1202−1221.
(63) Xie, W.; Xu, J.; Ding, Y.; Hu, P. Quantitative Studies of the Key Aspects in Selective Acetylene Hydrogenation on Pd(111) by Microkinetic Modeling with Coverage Effects and Molecular Dynamics. *ACS Catal.* **2021**, *11* (7), 4094−4106.
(64) Xie, W.; Xu, J.; Chen, J.; Wang, H.; Hu, P. Achieving Theory-Experiment Parity for Activity and Selectivity in Heterogeneous Catalysis Using Microkinetic Modeling. *Acc. Chem. Res.* **2022**, *55* (9), 1237−1248.
(65) Yao, Z.; Guo, C.; Mao, Y.; Hu, P. Quantitative Determination of C-C Coupling Mechanisms and Detailed Analyses on the Activity and Selectivity for Fischer−Tropsch Synthesis on Co(0001): Microkinetic Modeling with Coverage Effects. *ACS Catal.* **2019**, *9* (7), 5957−5973.
(66) Perdew, J. P.; Burke, K.; Ernzerhof, M. Generalized Gradient Approximation Made Simple. *Phys. Rev. Lett.* **1996**, *77* (18), 3865−3868.
(67) Kresse, G.; Furthmüller, J. Efficiency of ab-initio total energy calculations for metals and semiconductors using a plane-wave basis set. *Comput. Mater. Sci.* **1996**, *6* (1), 15−50.
(68) Kresse, G.; Hafner, J. Ab initio molecular-dynamics simulation of the liquid-metal-amorphous-semiconductor transition in germanium. *Phys. Rev. B: Condens. Matter Mater. Phys.* **1994**, *49* (20), 14251−14269.
(69) Grimme, S.; Ehrlich, S.; Goerigk, L. Effect of the damping function in dispersion corrected density functional theory. *J. Comput. Chem.* **2011**, *32* (7), 1456−1465.
(70) Grimme, S.; Antony, J.; Ehrlich, S.; Krieg, H. A consistent and accurate ab initio parametrization of density functional dispersion correction (DFT-D) for the 94 elements H-Pu. *J. Chem. Phys.* **2010**, *132* (15), 154104.
(71) Wang, J.; Guo, B.; Sun, J.; Zhou, Y.; Zhao, C.; Wei, Z.; Guo, J. Cooperative hydrogen evolution reaction combining $Cu_{2+1}O$ and Ru active sites. *Appl. Catal., B* **2023**, *324*, 122169.
(72) Cao, Y.; Meng, Y.; Wu, Y.; Huang, H.; Zhong, W.; Shen, Z.; Xia, Q.; Wang, Y.; Li, X. Metal-free boron nanosheet as "buffer electron pool" for urea and ethanol synthesis via C-N and C-C coupling. *J. Mater. Chem. A* **2022**, *10* (44), 23843−23853.
(73) Cao, Y.; Meng, Y.; Wu, Y.; Shen, Z.; Xia, Q.; Huang, H.; Lang, J. P.; Gu, H.; Wang, Y.; Li, X. Regulation of the Coordination Structures of Transition Metals on Nitrogen-Doped Carbon Nanotubes for Electrochemical CO_2 Reduction. *Inorg. Chem.* **2022**, *61* (47), 18957−18969.
(74) Cheng, J.; Song, T.; Hu, P.; Lok, C. M.; Ellis, P.; French, S. A density functional theory study of the α-olefin selectivity in Fischer−Tropsch synthesis. *J. Catal.* **2008**, *255* (1), 20−28.
(75) Mao, Y.; Hu, P. Identification of the active sites and mechanism for partial methane oxidation to methanol over copper-exchanged CHA zeolites. *Sci. China: Chem.* **2020**, *63* (6), 850−859.
(76) Kresse, G.; Joubert, D. From ultrasoft pseudopotentials to the projector augmented-wave method. *Phys. Rev. B* **1999**, *59* (3), 1758−1775.
(77) Blochl, P. E.; Jepsen, O.; Andersen, O. K. Improved tetrahedron method for Brillouin-zone integrations. *Phys. Rev. B: Condens. Matter Mater. Phys.* **1994**, *49* (23), 16223−16233.

https://doi.org/10.1021/acscatal.3c03893
ACS Catal. 2023, 13, 15054−15073

(78) Weaver, J. F. Surface chemistry of late transition metal oxides. *Chem. Rev.* **2013**, *113* (6), 4164−4215.
(79) Wang, F.; Xia, C.; de Visser, S. P.; Wang, Y. How Does the Oxidation State of Palladium Surfaces Affect the Reactivity and Selectivity of Direct Synthesis of Hydrogen Peroxide from Hydrogen and Oxygen Gases? A Density Functional Study. *J. Am. Chem. Soc.* **2019**, *141* (2), 901−910.
(80) Rogal, J.; Reuter, K.; Scheffler, M. Thermodynamic stability of PdO surfaces. *Phys. Rev. B* **2004**, *69* (7), 075421.
(81) Monkhorst, H. J.; Pack, J. D. Special points for Brillouin-zone integrations. *Phys. Rev. B* **1976**, *13* (12), 5188−5192.
(82) Alavi, A.; Hu, P.; Deutsch, T.; Silvestrelli, P. L.; Hutter, J. CO Oxidation on Pt(111): An Ab Initio Density Functional Theory Study. *Phys. Rev. Lett.* **1998**, *80* (16), 3650−3653.
(83) Liu, Z. P.; Hu, P. General rules for predicting where a catalytic reaction should occur on metal surfaces: a density functional theory study of C-H and C-O bond breaking/making on flat, stepped, and kinked metal surfaces. *J. Am. Chem. Soc.* **2003**, *125* (7), 1958−1967.
(84) Michaelides, A.; Liu, Z. P.; Zhang, C. J.; Alavi, A.; King, D. A.; Hu, P. Identification of general linear relationships between activation energies and enthalpy changes for dissociation reactions at surfaces. *J. Am. Chem. Soc.* **2003**, *125* (13), 3704−3705.
(85) Cortright, R. D.; Dumesic, J. A. Kinetics of heterogeneous catalytic reactions: Analysis of reaction schemes. *Adv. Catal.* **2001**, *46*, 161−264.
(86) V, D.; Roy; Keith, T.; Millam, J.. *GaussView*; Semichem Inc.: Shawnee Mission, KS, 2009.
(87) Lee, C.; Yang, W.; Parr, R. G. Development of the Colle-Salvetti correlation-energy formula into a functional of the electron density. *Phys. Rev. B: Condens. Matter Mater. Phys.* **1988**, *37* (2), 785−789.
(88) Becke, A. D. Density-functional thermochemistry. III. The role of exact exchange. *J. Chem. Phys.* **1993**, *98* (7), 5648−5652.
(89) Grabow, L. C.; Hvolbæk, B.; Falsig, H.; Nørskov, J. K. Search Directions for Direct H_2O_2 Synthesis Catalysts Starting from Au12 Nanoclusters. *Top. Catal.* **2012**, *55* (5−6), 336−344.
(90) Rankin, R. B.; Greeley, J. Trends in Selective Hydrogen Peroxide Production on Transition Metal Surfaces from First Principles. *ACS Catal.* **2012**, *2* (12), 2664−2672.
(91) Chen, J.-F.; Mao, Y.; Wang, H.-F.; Hu, P. Reversibility Iteration Method for Understanding Reaction Networks and for Solving Microkinetics in Heterogeneous Catalysis. *ACS Catal.* **2016**, *6* (10), 7078−7087.
(92) Grabow, L. C.; Hvolbæk, B.; Norskov, J. K. Understanding Trends in Catalytic Activity: The Effect of Adsorbate-Adsorbate Interactions for CO Oxidation Over Transition Metals. *Top. Catal.* **2010**, *53* (5−6), 298−310.
(93) Lausche, A. C.; Medford, A. J.; Khan, T. S.; Xu, Y.; Bligaard, T.; Abild-Pedersen, F.; Nørskov, J. K.; Studt, F. On the effect of coverage-dependent adsorbate-adsorbate interactions for CO methanation on transition metal surfaces. *J. Catal.* **2013**, *307*, 275−282.
(94) Reuter, K.; Scheffler, M. Composition, structure, and stability of RuO_2(110) as a function of oxygen pressure. *Phys. Rev. B* **2001**, *65* (3), 035406.
(95) Reuter, K.; Scheffler, M. Composition and structure of the RuO_2(110) surface in an O_2 and CO environment: Implications for the catalytic formation of CO_2. *Phys. Rev. B* **2003**, *68* (4), 045407.
(96) Reuter, K.; Frenkel, D.; Scheffler, M. The steady state of heterogeneous catalysis, studied by first-principles statistical mechanics. *Phys. Rev. Lett.* **2004**, *93* (11), 116105.
(97) Reuter, K.; Scheffler, M. Oxide formation at the surface of late 4d transition metals: insights from first-principles atomistic thermodynamics. *Appl. Phys. A: Mater. Sci. Process.* **2004**, *78* (6), 793−798.
(98) Soon, A.; Todorova, M.; Delley, B.; Stampfl, C. Oxygen adsorption and stability of surface oxides on Cu(111): A first-principles investigation. *Phys. Rev. B* **2006**, *73* (16), 165424.
(99) Chen, L.; Medlin, J. W.; Grönbeck, H. On the Reaction Mechanism of Direct H_2O_2 Formation over Pd Catalysts. *ACS Catal.* **2021**, *11* (5), 2735−2745.
(100) Campbell, C. T. Future Directions and Industrial Perspectives Micro- and macro-kinetics: Their relationship in heterogeneous catalysis. *Top. Catal.* **1994**, *1* (3−4), 353−366.
(101) Campbell, C. T. Finding the Rate-Determining Step in a Mechanism. *J. Catal.* **2001**, *204* (2), 520−524.
(102) Stegelmann, C.; Andreasen, A.; Campbell, C. T. Degree of Rate Control: How Much the Energies of Intermediates and Transition States Control Rates. *J. Am. Chem. Soc.* **2009**, *131* (37), 13563.
(103) Campbell, C. T. The Degree of Rate Control: A Powerful Tool for Catalysis Research. *ACS Catal.* **2017**, *7* (4), 2770−2779.
(104) Rogal, J.; Reuter, K.; Scheffler, M. CO oxidation at Pd(100): A first-principles constrained thermodynamics study. *Phys. Rev. B* **2007**, *75* (20), 205433.
(105) Filot, I. A. W.; Broos, R. J. P.; van Rijn, J. P. M.; van Heugten, G. J. H. A.; van Santen, R. A.; Hensen, E. J. M. First-Principles-Based Microkinetics Simulations of Synthesis Gas Conversion on a Stepped Rhodium Surface. *ACS Catal.* **2015**, *5* (9), 5453−5467.
(106) Bianchi, G.; Mazza, F.; Mussini, T. Catalytic decomposition of acid hydrogen peroxide solutions on platinum, iridium, palladium and gold surfaces. *Electrochim. Acta* **1962**, *7* (4), 457−473.
(107) Serra-Maia, R.; Bellier, M.; Chastka, S.; Tranhuu, K.; Subowo, A.; Rimstidt, J. D.; Usov, P. M.; Morris, A. J.; Michel, F. M. Mechanism and Kinetics of Hydrogen Peroxide Decomposition on Platinum Nanocatalysts. *ACS Appl. Mater. Interfaces* **2018**, *10* (25), 21224−21234.
(108) Adams, J. S.; Kromer, M. L.; Rodriguez-Lopez, J.; Flaherty, D. W. Unifying Concepts in Electro- and Thermocatalysis toward Hydrogen Peroxide Production. *J. Am. Chem. Soc.* **2021**, *143* (21), 7940−7957.
(109) Wilson, N. M.; Schröder, J.; Priyadarshini, P.; Bregante, D. T.; Kunz, S.; Flaherty, D. W. Direct synthesis of H_2O_2 on PdZn nanoparticles: The impact of electronic modifications and heterogeneity of active sites. *J. Catal.* **2018**, *368*, 261−274.
(110) Wilson, N. M.; Priyadarshini, P.; Kunz, S.; Flaherty, D. W. Direct synthesis of H_2O_2 on Pd and AuxPd1 clusters: Understanding the effects of alloying Pd with Au. *J. Catal.* **2018**, *357*, 163−175.
(111) Voloshin, Y.; Halder, R.; Lawal, A. Kinetics of hydrogen peroxide synthesis by direct combination of H_2 and O_2 in a microreactor. *Catal. Today* **2007**, *125* (1−2), 40−47.
(112) Menegazzo, F.; Signoretto, M.; Ghedini, E.; Strukul, G. Looking for the "Dream Catalyst" for Hydrogen Peroxide Production from Hydrogen and Oxygen. *Catalysts* **2019**, *9* (3), 251.
(113) Liu, Q.; Lunsford, J. H. Controlling factors in the direct formation of H_2O_2 from H_2 and O_2 over a Pd/SiO_2 catalyst in ethanol. *Appl. Catal., A* **2006**, *314* (1), 94−100.
(114) Yook, S.; Shin, H.; Kim, H.; Choi, M. Selective Dissociation of Dihydrogen over Dioxygen on a Hindered Platinum Surface for the Direct Synthesis of Hydrogen Peroxide. *ChemCatChem* **2014**, *6* (10), 2836−2842.
(115) Pashkova, A.; Greiner, L.; Krtschil, U.; Hofmann, C.; Zapf, R. Direct synthesis of hydrogen peroxide over supported Pd catalysts: Turning to dense CO_2 as an alternative solvent. *Appl. Catal., A* **2013**, *464−465*, 281−287.
(116) Biasi, P.; Gemo, N.; Hernández Carucci, J. R.; Eränen, K.; Canu, P.; Salmi, T. O. Kinetics and Mechanism of H_2O_2 Direct Synthesis over a Pd/C Catalyst in a Batch Reactor. *Ind. Eng. Chem. Res.* **2012**, *51* (26), 8903−8912.
(117) Gemo, N.; Biasi, P.; Canu, P.; Salmi, T. O. Mass transfer and kinetics of H_2O_2 direct synthesis in a batch slurry reactor. *Chem. Eng. J.* **2012**, *207−208*, 539−551.

https://doi.org/10.1021/acscatal.3c03893
ACS Catal. 2023, 13, 15054−15073